JPhys Materials

PAPER • OPEN ACCESS

Charge transfer state characterization and voltage losses of organic solar cells

To cite this article: Anna Jungbluth *et al* 2022 *J. Phys. Mater.* **5** 024002

IOP Publishing J. Phys. Mater. 5 (2022) 024002 https://doi.org/10.1088/2515-7639/ac44d9

Journal of Physics: Materials

OPEN ACCESS

RECEIVED
31 August 2021

REVISED
3 December 2021

ACCEPTED FOR PUBLICATION
20 December 2021

PUBLISHED
26 January 2022

PAPER

Charge transfer state characterization and voltage losses of organic solar cells

Anna Jungbluth[1], **Pascal Kaienburg**[1] **and Moritz Riede**[*]

Clarendon Laboratory, Department of Physics, University of Oxford, Parks Road, OX1 3PU Oxford, United Kingdom

[1] These authors contributed equally.

[*] Author to whom any correspondence should be addressed.

E-mail: moritz.riede@physics.ox.ac.uk

Keywords: organic solar cells, charge transfer states, voltage losses, Marcus theory, Marcus-Levich-Jortner theory, three-state models

Abstract

A correct determination of voltage losses is crucial for the development of organic solar cells (OSCs) with improved performance. This requires an in-depth understanding of the properties of interfacial charge transfer (CT) states, which not only set the upper limit for the open-circuit voltage of a system, but also govern radiative and non-radiative recombination processes. Over the last decade, different approaches have emerged to classify voltage losses in OSCs that rely on a generic detailed balance approach or additionally include CT state parameters that are specific to OSCs. In the latter case, a correct determination of CT state properties is paramount. In this work, we summarize the different frameworks used today to calculate voltage losses and provide an in-depth discussion of the currently most important models used to characterize CT state properties from absorption and emission data of organic thin films and solar cells. We also address practical concerns during the data recording, analysis, and fitting process. Departing from the classical two-state Marcus theory approach, we discuss the importance of quantized molecular vibrations and energetic hybridization effects in organic donor-acceptor systems with the goal to providing the reader with a detailed understanding of when each model is most appropriate.

1. Introduction

Improvements in the open-circuit voltage (V_{oc}) have been integral to the success story of organic solar cells (OSCs) and are arguably the main target of OSC material discovery. The evolving understanding of the underlying physics and processes that govern the V_{oc} were, and continue to be, key to drive innovation in the design and synthesis of novel molecules. Until the 1980s, the first reported OSCs [1, 2] were based on an absorber layer consisting of a single molecular species. Such devices reached high V_{oc}, which is largely governed by the work function of the electrodes, but photocurrents were low because of inefficient dissociation of excitons that are formed upon light absorption by an organic molecule. The introduction of a second molecular species [3], creating a type II heterojunction at the interface between the electron donor and acceptor molecule (figure 1(a)), facilitated efficient exciton dissociation. However, the energetic offset at the heterojunction decreased the energy of the resulting free charge carriers. In other words, V_{oc} was sacrificed for the short-circuit current density (J_{sc}), resulting in a net improvement of power conversion efficiency (PCE). Rather than a planar donor-acceptor interface, today's best performing OSCs apply a bulk-heterojunction (BHJ) [4, 5] morphology where the donor and acceptor molecules are intermixed on a scale of ∼10 nm mandated by the exciton diffusion length of the used materials. Again, the benefit of this morphology is a higher photocurrent. Since these early developments, OSC researchers made great efforts to recover the comparably high open-circuit voltages for BHJ devices that were reached with the early single-component absorber layers, while maintaining high J_{sc}—an effort that was deemed complete only recently [6]. However, even today, a reduced V_{oc} remains a major loss factor in OSCs [7, 8].

While correlations between V_{oc} and electrode work functions were also observed in BHJs [9] by applying suitable and versatile contact configurations, the interface energetics of the electron donor and acceptor

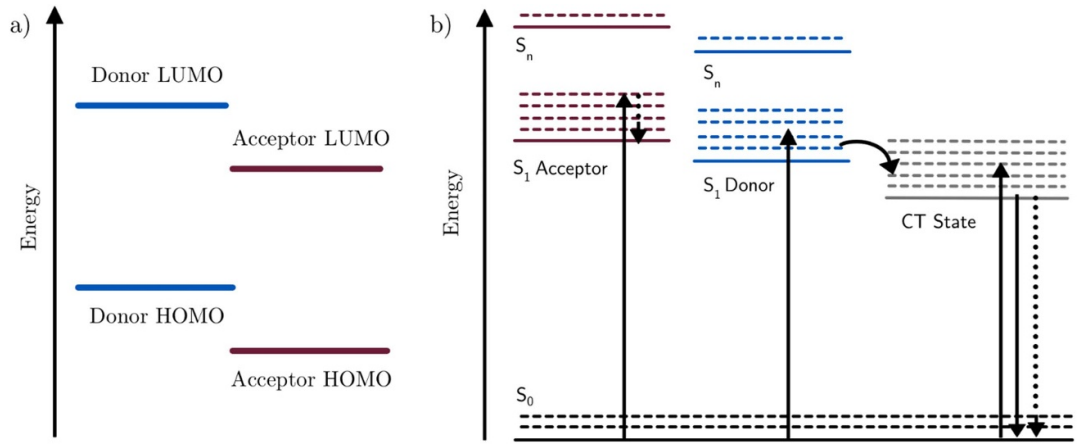

Figure 1. (a) Type II heterojunction based on (usually independently determined) donor/acceptor HOMO and LUMO levels reflecting single particle states. (b) Jablonski diagram depicting the ground state (S_0) and singlet states ($S_1 \ldots S_n$) of the donor and acceptor molecules, as well as the interfacial CT state (all two-particle states). Depending on the material system, either the donor or acceptor molecules show the lower singlet energy. The dashed lines represent vibrational energy levels. Vertical solid arrows represent absorption and radiative emission between the excited and ground states. Dotted arrows depict non-radiative recombination pathways.

molecules were found to dominate $\boldsymbol{V_{oc}}$ [10]. From roughly 1994–2015, researchers employed fullerene $\boldsymbol{C_{60}}$ or solubilised fullerene derivatives as acceptor molecules to achieve high power conversion efficiencies, eventually exceeding 10% [7]. Despite the wealth of possible donor molecules, a core requirement was that the donor molecular energy levels showed an offset to the fullerene energy levels of at least 300 mV [10]. Work on reducing this energetic offset, as mapped out by Scharber *et al* [10], was hugely successful [11] but ultimately limited by the minimum energetic offset at the heterojunction, which results in a significant voltage loss [7, 12, 13]. In addition, describing voltages losses in terms of the highest occupied molecular orbital (HOMO) and lowest unoccupied molecular orbital (LUMO) of unblended molecules is not entirely representative as these values are typically measured at the surface of a pristine film. This approach neglects any interactions at the (buried) donor-acceptor interface, such as polarization, electrostatic dipoles, quadrupole interactions, and—representing single particle states—exciton binding energies [14]. In fact, the role of a LUMO and/or HOMO offset at the donor-acceptor interface for exciton separation remains a topic of debate [15, 16].

Moving the focus away from the molecular energy levels of isolated molecules, a more accurate and meaningful physical description for the processes governing $\boldsymbol{V_{oc}}$ emerged around 2008 [17–21] that focused on the interface energetics of donor and acceptor molecules in the absorber layer of full solar cell device stacks. In particular, the charge transfer (CT) state that forms between donor and acceptor molecules was shown to correlate well with $\boldsymbol{V_{oc}}$ [17, 19]. The more heuristic approach of tailoring the donor HOMO—acceptor LUMO difference had its merits [11, 22] because the energy levels of isolated molecules strongly influence the CT state energy [23]. However, knowledge on individual energy levels does not suffice to characterize CT states since interfacial interactions are not captured accurately. Several milestone publications [20, 21, 24] discussed the nature and detailed properties of the CT state and its influence on the $\boldsymbol{V_{oc}}$. The type II heterojunction picture (figure 1(a)), highlighting the 'driving force' for exciton dissociation as the donor HOMO—acceptor LUMO difference, was replaced by a picture where the difference between the CT state and the lowest lying singlet $\boldsymbol{S_1}$ becomes important (figure 1(b)). In 2015, highly efficient non-fullerene acceptors (NFAs) emerged, some of which do not show any measurable offset between the CT state and $\boldsymbol{S_1}$, leading to efficiencies of most recently up to 18% [25]. Notably, a significant energetic offset results in a reduced (quenched) photoluminescence (PL) intensity compared to the single material. A quenched PL was for a long time used as an indicator for finding promising molecules during material screening processes. The newly achieved performance enhancements of low-offset systems with significant PL deems this approach unfit and suggests that researchers could have dismissed promising material combinations in the past.

This brief history of the $\boldsymbol{V_{oc}}$ in OSCs illustrates why understanding CT states is hugely important for progress in the field. As of today, large losses in $\boldsymbol{V_{oc}}$ remain the major drawback of OSCs compared to other inorganic solar cell technologies such as silicon or (hybrid) perovskites [26]. The CT state and associated vibronic transitions are distinguished features of OSCs and ultimately responsible for this lag in performance. Consequently, various CT state models were developed, and their adequacy was argued for

certain materials and under certain conditions, creating an extensive body of literature. In parallel, experimental characterization of CT states in OSCs from novel, well-performing molecules via light absorption and emission-based techniques has become more commonplace to gain a comprehensive understanding on voltage losses. CT state properties can act as a quality indicator or even figure of merit for molecules. However, analysing and interpreting the data is not straightforward, especially when absolute values rather than trends are of interest.

In this review, we provide a critical discussion of both established and novel approaches to characterize CT states and voltage losses of OSCs. We discuss experimental considerations and the underlying physical assumptions of the different approaches and aim to provide a framework for deciding which approach is most appropriate in different contexts. Our goal is to present a comprehensive picture on measurement techniques and help the reader develop an understanding of the magnitude and importance of typical sources of error in experimental measurements and analysis approaches. This discussion is relevant for a range of material systems and OSC technologies and applies to both fullerenes as well as NFA-based systems with low driving force. Solution-processed NFA:polymer blends constitute today's most efficient lab-based OSCs. However, fullerenes remain the state-of-the-art acceptor molecules for small molecule thermal vacuum-evaporated solar cells with high industrial significance.

In section 2, we provide an overview of experimental measurements of CT states and voltage losses. Section 3 focusses on reciprocity theorems relating emission and absorption in solar cells. Section 4 expands on this understanding to discuss two major frameworks for determining voltage losses, namely the detailed balance (DB) approach, and calculating voltage losses in an energetic state picture using CT state properties. Finally, section 5 focusses on an in-depth discussion of the different models used to describe CT processes and how these models are being applied to fit CT states. A final discussion and recommendations on when to apply each approach are provided in section 6.

2. Experimental techniques to measure CT states and voltage losses

The experimental techniques to investigate voltage losses at open circuit and CT states are largely the same and fall into two classes of spectroscopic techniques based on either light emission or light absorption. Energetically, CT states are the lowest absorbing and emitting states in a system [20, 21]. This low energy spectral region is not only relevant for CT state characterization but also for voltage loss analysis. Data from absorption and emission measurements are connected (or even interchangeable) via reciprocity theorems [27, 28], but it is generally advantageous to combine absorption and emission measurements to obtain the most reliable results.

Measurements are mostly done on full devices (i.e. solar cells with top and bottom electrodes), or films of just the material blends on a substrate like glass or quartz. Solar cell measurements detect light emission upon current injection (electroluminescence/EL) or solar cell photocurrent upon illumination (sensitive external quantum efficiency/EQE, Fourier-transform photocurrent spectroscopy/FTPS). Measurements on films require photo-injection of charges (photoluminescence/PL) for subsequent emission detection or the direct measure of absorption upon illumination (photothermal deflection spectroscopy/PDS). Another option is to measure photoconductivity upon absorption with co-planar (non-diode) electrical contacts (constant photocurrent measurements/CPMs).

In this section, we briefly highlight some of the most common techniques used to determine CT state properties and voltage losses, highlighting several practical considerations, followed by a discussion of reciprocity and its application to OSCs.

2.1. External quantum efficiency

The EQE expresses the spectral dependence of the number of charge carrier pairs, collected in the device's external circuit, per incident photon ($\boldsymbol{EQE} = \frac{electron-holepairs/sec}{photons/sec}$). EQE setups [29] are a standard tool in the characterization of solar cells to investigate the spectrally dependent photocurrent and are needed for any mismatch correction [30]. Since absorption from the ground into the CT state is weak [21, 31], EQE measurements need to be performed at increased sensitivity to obtain a large enough dynamic range to resolve the CT state peak [32–34]. Higher sensitivities are achieved by using optical long-pass filters and lock-in amplifiers with dynamically controlled integration times. Depending on the strength of the optical transition, sensitivities of around 10^{-3} might suffice to detect CT state absorption but likely show substantial instrument noise in the region of interest. Reference [34] provides an excellent overview of further experimental improvements to measure EQE spectra down to a signal strength of $10^{-8} - 10^{-10}$.

Sensitive EQE measurements are arguably one of the most common experimental techniques to characterize CT states. FTPS [35–37] is another method to probe the EQE in the sub-gap region of a solar cell with high sensitivity. In comparison to EQE measurements, which use monochromatic light, FTPS

applies white light to the device under testing and spectral information is obtained through interferometry. Using a Fourier-transform infrared spectrometer, the intensity of different wavelengths of the white light are modulated periodically, and the resulting interferogram of the photocurrent is demodulated through Fourier transform analysis. With this, FTPS provides relative EQE values.

2.2. Absorptance

PDS [31, 37, 38] directly measures the (relative) absorptance of a thin film by detecting heat generated from the absorption of incident light and subsequent thermalization. The thin-film sample is placed in a cuvette filled with a liquid whose refractive index is strongly temperature dependent. The change in refractive index of the liquid upon heating, caused by absorption and thermalization in the thin film, is probed via the deflection of a laser beam that is directed parallelly to the sample and perpendicularly to the incident monochromatic light.

Instead of using a solar cell architecture and measuring the EQE, a variation of FTPS probes the photoconductivity [39, 40]. A film is deposited on glass with two contacts of the same metal placed millimetres apart to yield a co-planar configuration. In this configuration there is no built-in field and instead a high voltage is applied across the contacts to provide an electric field driving the charge carriers. For 100 V and 1 mm contact distance the electric field is 10^5 $\boldsymbol{V/m}$ compared to 10^7 $\boldsymbol{V/m}$ for a solar cell with 1 V built-in voltage and 100 nm thick absorber. The same co-planar geometry can be used for CPMs [41]. Here, a monochromatic light beam is directed at the sample, covering the entire gap between the electrodes, and the wavelength-dependent intensity that produces a constant photocurrent is recorded. The single-carrier photocurrent measured in this FTPS-variant and CPM is—assuming a wavelength-independent ratio of photon absorbed to carrier collected—also proportional to the absorptance.

2.3. Luminescence measurements

EL spectroscopy measurements [42] detect light emission after electrical injection of charge carriers into a device via an external circuit. During EL measurements, the solar cell is thus operated as a light emitting diode (LED). In OSCs, emission typically occurs via the CT state [19–21], making EL spectroscopy a powerful tool to study CT states [19, 43–45] and thus, in addition to sensitive EQE, a focus technique of this review. During measurements either the injected current or the applied voltage is kept constant and changes in the other parameter are recorded to detect heating or degradation of the sample. High voltages or currents can lead to well-defined peaks with high dynamic range but cause heating of the sample as observed by peak shifts of the spectra. In addition, with increasing voltage, emissions from higher lying states may be observed [19, 44]. Consequently, a balance needs to be struck to find optimal measurement conditions to measure stable and well-resolved CT state emission. Regarding signal detection, more than one detector might be needed to cover the full spectral range of interest as emission is often lower in energy than the band gap of silicon, a standard detector material. As a side note, the output signal of spectrometers is typically proportional $\frac{W}{nm}$, whose conversion into $\frac{\#\,photons}{eV}$ yields a factor $\boldsymbol{E}^3$.

PL spectroscopy [46] is the corresponding technique to measure emission of blend films but has been performed on full devices as well [47]. A laser is used to photoexcite excitons in the film which may recombine radiatively. Unblended organic semiconductors generally show strong PL emission because the excitons quickly recombine radiatively. In fullerene-based blends, the intensity of emission is reduced (quenched) [48] compared to unblended films since excitons are split via CT states which have much lower radiative recombination yields. High-efficiency NFA-based blends that exhibit low voltage losses can show considerable light emission upon photoexcitation [47].

2.4. Current–voltage measurements

Current density-voltage (J-V) characteristics are needed in the context of voltage loss analyses, which rely on values of the open-circuit voltage ($\boldsymbol{V_{oc}}$) and the short-circuit current density ($\boldsymbol{J_{sc}}$). The most accurate way to determine $\boldsymbol{J_{sc}}$ is a spectrally mismatch corrected solar simulator measurement [30] which accounts for an imperfectly simulated AM1.5 g spectrum as well as differences in the spectral responses of the calibration cell and the measured OSC, and only relies on relative EQE spectra. The alternative way of calculating the $\boldsymbol{J_{sc}}$ directly from the EQE via

$$J_{sc} = q \int_0^\infty EQE \cdot \phi_{AM1.5} dE \tag{1}$$

where q is the elementary charge, E is the photon energy, and $\phi_{AM1.5}$ is the photon flux corresponding to the AM 1.5 g spectrum with 100 mW cm^{-2}, has the underlying issue that there is uncertainty in measuring the absolute EQE and is thus not recommended except when calculating the radiative V_{oc} as discussed later.

Errors may, for example, arise from imperfect optical alignment, from measuring at low charge carrier densities if no bias illumination is used, or from uncertainties in determining the photovoltaic active area. However, equation (1) can be used to obtain accurate absolute EQE values by scaling the spectrum so it matches the mismatch corrected J_{sc}.

Spectral mismatch correction only addresses linear effects and a lamp spectrum close to the AM1.5 g spectrum should be used, i.e. something commonly available white LEDs do not achieve. While spectral mismatch correction provides an accurate value for J_{sc}, it does not correct the V_{oc}, which is likely to cause uncertainties in the determination of voltage losses. Thus, the recommended way of measuring the J-V behaviour is with an illumination intensity that produces the mismatch corrected J_{sc} value. This can be achieved by tuning the lamp current until a measured reference cell produces a current corresponding to 100 mW cm^{-2} incident light intensity. Furthermore, the V_{oc} is sensitive to the temperature of the absorber layer. Assuming the absorber temperature equals that of the substrate, the substrate is ideally held at a controlled temperature, such as 25 °C (Standard Testing Condition) or the same room temperature as during EQE and EL measurements to keep conditions consistent. Additionally, since efficient OSCs show little to no hysteresis, quick scans with sweep direction from V_{oc} to J_{sc} minimize heat generation and are therefore the suggested method to determine V_{oc}.

2.5. Relating experiment and theory

Since $\boldsymbol{V_{oc}}$ is a quantity related to a photovoltaic device, accurate voltage loss analysis requires device measurements of current density-voltage characteristics (J-V), sensitive EQE, and/or EL. The analysis of CT states, on the other hand, in the first instance refers to properties of the absorber material blend rather than the device: different CT theories discussed in section 5 provide optical transition rates between the ground and CT state as well as information of absorption coefficients and emission behaviour.

Rather than directly measuring the transition rates or material blend properties like absorption and emission coefficients, the methods discussed above probe film properties, like absorptance $\boldsymbol{a}$, or device properties, like the EQE. The corresponding material properties, e.g. the absorption coefficient, are obtained by applying a suitable optical model for thin films [49–51]. For device properties, an additional electronic model is also needed, although this is usually assumed to be a simple scaling factor—e.g. charge carrier collection efficiency is assumed to be independent of photon energy in the region of interest [21], thus EQE$\sim \boldsymbol{a}$. With the CT states falling into the region of weak-absorption, multiple reflection and interference effects occur in addition to Lambert-Beer absorption. Simple optical models equating the absorptance as $\boldsymbol{\alpha = \alpha d}$ (or $\boldsymbol{a = 2\alpha d}$ in a device with reflective back contacts) may therefore introduce significant errors as discussed in more detail in section 5. Numerical optical simulations, performed for example through transfer matrix methods [52], allow to take optical phenomena like interference effects into account.

While the optics are simpler in thin-films than in devices, device measurements often offer higher dynamic range for OSCs—compare EL with PL and sensitive EQE with PDS. They have the additional advantage that the measurements can be performed on the same device that is used for J-V characterization, whereas films might, for example, show different microstructural properties compared to full solar cells due to changes in the substrates and layer stacks. Consequently, solar cells are commonly used to study CT states and are thus the emphasis of this review.

As mentioned in the respective sections, many of the discussed methods provide relative values that require scaling to the absolute value via a complementary technique such that both measurement curves align. For absorptance, this can be Transmission-Reflection or ellipsometry measurements, and for FTPS this can be standard EQE measurements. Emission experiments typically yield relative values that can be scaled by applying reciprocity relations. Note, that there are ways to measure emission in absolute values [20, 53] commonly denoted as PL Quantum Yield [54] and LED quantum efficiency. While relative values suffice to fit spectral features such as the CT state energy and relaxation energy, absolute values are needed to determine voltage losses or the oscillator strength of the optical transition between the ground and CT state as discussed in more detail later.

3. Reciprocity in OSCs

There are multiple reciprocity relations, based on the principle of DB [53], that quantitatively link a process to its reverse action. Examples are Würfel's optical reciprocity relating absorptance and PL [28], and Donolato's electronic reciprocity relating charge injection and collection [55]. Rau's optoelectronic reciprocity theorems [27] combine the two and relate (spectral and angular) EL and EQE, as well as LED quantum efficiency and non-radiative voltage losses.

EQE and EL spectra are linked via the black body spectrum $\phi_{bb}(T,\ E)$ and a voltage-dependent factor

$$\delta\phi_{em}(E) = EQE(E)\cdot\phi_{bb}(T,E)\cdot\left(e^{\frac{qV}{k_BT}}-1\right) \tag{2}$$

with the excess emission $\delta\phi_{em}$ upon charge injection (compared to emission in the dark without applied bias V). Here, T is the temperature, E the photon energy, q the elementary charge, and k_B is Boltzmann's constant. When only a relative EL spectrum is recorded, collecting an unknown fraction of emitted photons, the scaling factor for the absolute spectrum can be recovered via equation (2) by converting the EL spectrum into an EQE spectrum and aligning it to the measured EQE. Note that in this procedure the voltage term is ignored as it is part of the proportionality factor between $\delta\phi_{em}(E)$ and $EQE(E)\,\phi_{bb}(T,E)$. Rau's reciprocity theorem therefore implies that the EQE and EL spectra contain the same information, when experimental considerations such as energetic range or sensitivity of signal detection are considered explicitly. Consequently, the EQE data calculated from EL measurements using equation (2) can often extend the measured EQE further into the sub-gap region.

The radiative saturation current density can be calculated as

$$J_0^{rad} = q\int_0^\infty EQE\cdot\phi_{bb}dE = q\int_0^\infty \delta\phi_{em}(E)\,dE \tag{3}$$

with the absolute (excess) emission $\delta\phi_{em}(E)$ obtained after scaling the relative EQE spectrum according to equation (2). Equation (4) yields the radiative open-circuit voltage

$$V_{oc}^{rad} = \frac{k_BT}{q}\ln\left(\frac{J_{sc}}{J_0^{rad}}\right) \tag{4}$$

describing the V_{oc} value in the best case of a non-ideal solar cell where the EQE is not a step-function, but only radiative recombination occurs. The difference between the V_{oc}^{rad} to the measured V_{oc} results from non-radiative voltage losses ΔV_{oc}^{nr} typically caused by phonon or vibration-mediated electronic transitions [24, 55]. Non-radiative voltage losses are related to the LED quantum efficiency Q_{LED}—the inverse ratio of the number of injected charge pairs that are converted into emitted photons—via another reciprocity theorem [27, 56, 57]

$$\Delta V_{oc}^{nr} = V_{oc}^{rad} - V_{oc} = \frac{k_BT}{q}ln\left(Q_{LED}^{-1}\right) = \frac{k_BT}{q}\ln\left(\frac{J_0}{J_0^{rad}}\right). \tag{5}$$

Rau's two reciprocity relations are quintessential throughout this review for drawing conclusions from EL and EQE spectra on CT state properties and for conducting meaningful and rigorous voltage loss analyses. It is therefore imperative to confirm the validity of these reciprocity relations in different measurement contexts.

Strictly speaking, Rau's reciprocity relations are only valid when recombination depends linearly on charge carrier density, which is not the case, e.g. for solar cells where the superposition principle [58] of the photocurrent being voltage-independent is violated. This is the case for OSCs and many other thin-film solar cells, and violations have been observed [59, 60]. Causes for reciprocity to be violated in OSCs include static disorder [61], optical interference [62], and, as predicted from simulations, low mobilities [60]. However, in practice, the reciprocity relations often hold well enough in OSCs [20, 63].

There are two relatively simple ways to test whether the reciprocity relations are fulfilled to a satisfactory degree [64]; (1) converting EL to EQE spectra—and vice versa—according to equation (2) and checking for agreement in the spectral region covered by both measurements, and (2) varying the injection current (or applied voltage) during EL measurements and confirming that the emission peak does not shift in the parameter range used for analysis. Additionally, the intensity of the measured EL peak should scale with voltage according to equation (2). An example of a thorough examination of the applicability of reciprocity relations can be found in [59].

Importantly, Joule heating during EL measurements may result in a different slope of the emission tail when comparing to the EQE where the absorber is at room temperature. This may be interpreted as a violation of the first reciprocity relation although it is merely a temperature effect that can be corrected by extracting the temperature from the EL emission tail [32, 65]. However, to avoid artefacts, it is preferable to work at low injection currents during EL measurements and only analyse data at such currents where reciprocity relations directly apply. As discussed in the experimental section, this requires striking a balance between EL signal intensity and injection current. Slight deviations from reciprocity might still be acceptable from a practical point of view [20, 65], but the resulting uncertainty in the extracted values should be kept in mind. Finally, if reciprocity relations are clearly violated, more sophisticated models [59, 61, 62] need be considered to interpret and relate EL and EQE spectra [59] and conduct voltage loss analyses [26].

4. Voltage loss analysis

As for many other PV technologies, voltage losses are a major contributor to non-ideal performance in OSCs, and in fact, are significantly higher for OSCs than for other well-performing technologies. The 'voltage losses' referred to earlier describe the difference between a reference energy, typically representing the optical gap (or absorption edge), and the open-circuit voltage $\Delta V = E_{\mathrm{ref}} - V_{\mathrm{oc}}$ at Standard Testing Conditions (100 mW cm^{-2}, 25 °C junction/cell temperature, AM1.5 g spectrum). A deeper understanding on the origin of voltage losses continues to be invaluable for improving OSCs and the molecules involved.

We discuss two primary methods of giving a more detailed account of voltage losses in OSCs that are commonly used in literature. Both methods split ΔV into different loss contributions related to their different origins. The detailed balance 'DB' method is purely based on the thermodynamics of light in the context of solar cells [26, 27], and is as such a general framework that applies equally to organic and inorganic solar cells. The 'energetic states' method is based on DB but includes additional physics specific to OSCs [14], i.e. an explicit consideration of the CT state.

4.1. Choice of reference energy

For OSCs, the 'optical band gap' reflecting the absorption edge is commonly used as reference energy in voltage loss analysis. While it is clearly understood that this refers to the spectral region where strong absorption commences, the issue here is that there is no clearly defined single energy value for an optical gap in OSCs or, in fact, any other real solar cell [12]. Various approaches to determine the reference energy are applied in literature. The chosen approach should strike a balance between being physical meaningful, fit for purpose, and accounting for practical concerns such as ease of use and reproducibility of measurements and analysis. Physically accurate choices of reference energies to estimate voltage losses are discussed in the following paragraphs. Ultimately, it is important to use a consistent methodology for determining reference energies when comparing samples. To achieve consistency, this might require the re-analysis of reported data if the raw data is published alongside manuscripts. For this, easy access to literature data, ideally through open data policies, is paramount.

As part of the voltage loss analysis in the DB picture, based on solar cell device properties, the determination of the reference energy E_{ref} via the EQE is useful [12, 14, 26] as EQE spectra are commonly measured and reported, allowing for comparison across literature data and PV technologies [26]. The reference energy as determined via the inflection point of the EQE edge can be understood as a 'photovoltaic band gap' E_g^{PV} referring to a device rather than a material property [26]. The inflection point approach is assessed easily, even if it carries an uncertainty of about 10 meV. This uncertainty can be reduced by averaging over the absorption edge [26] or fitting a sigmoid function to the data [66] as encouraged by the research community [67].

The energetic state picture emphasizes the energetic position of the CT state relative to the 'optical gap', defined as the lowest absorbing singlet E_{S1}, and is thus chosen as reference energy E_{ref} [14]. E_{S1} can be determined by fitting the EQE spectrum of the solar cell using Gaussian functions as described in more detail in section 5. Alternatively, E_{S1} can be determined from a film or device of the neat (unblended) material with the lower optical gap by fitting absorption and emission spectra or determining the intersection point of the two. However, this approach requires a careful consideration of any spectral shifts between blended and neat films, as a significant difference would make the determination of E_{S1} from neat films unsuitable. Such shifts may result from the different chemical and morphological environments of the molecules causing a variation in polarization and electrostatic interactions.

Note that the commonly used absorption onset, determined from the x-axis intersection of a tangent, chosen at some point of the (often non-linear) edge of an absorption or EQE spectrum, is neither physically meaningful nor very reproducible [12] and should be avoided as it can even produce negative voltage losses. The same applies for the Tauc plot, which is often applied to characterize direct transitions in crystalline inorganic semiconductors and relies on fitting a tangent. Also, the non-optical definition of the band gap via the difference of donor ionization energy and acceptor electron affinity lacks physical meaning and accuracy [14], although it can be used as a proxy during material development [12]. Further discussions on the band gap of OSCs can be found elsewhere [12, 14, 26].

4.2. Radiative open-circuit voltage

The V_{oc}^{rad}, introduced in the context of the reciprocity relations in section 3, is central to both the DB and energetic state picture to determine voltage losses. It is a robust and clearly defined quantity that does not depend on any fitting approach or consensus definition. However, one needs to ensure that all significant contributions to the integrals in equation (4) are accounted for, which requires sufficiently sensitive setups to achieve high dynamic range of the data.

The integral boundaries of energy—which in theory should be $(0, \infty)$—must be chosen to include as much of the signal as possible while excluding the noise floor (a noisy signal itself is less problematic for the integration). Comparing and visualizing the terms in the integral ($\delta\phi_{em}$ or $EQE \cdot \phi_{bb}$) is helpful to check whether contributions close to the integral boundaries are significant. Similarly, the integral boundaries can be varied up to the maximum range determined by the noise floor to observe resulting changes in the integrated value. If values close to the maximum boundaries contribute significantly, or the integrated value does not show saturation upon varying the boundaries, the calculated V_{oc}^{rad} value must be interpreted cautiously.

Within the reciprocity theorem [27], equation (4) approximates the photocurrent at V_{oc} as the short-circuit current. The photocurrent density J_{ph} is defined as the difference between current density under illumination and the dark current density, at V_{oc}. OSCs do not strictly match the assumptions of the reciprocity theorem and $J_{ph}(V_{oc})$ differs from $J_{ph}(V = 0V) \equiv J_{sc}$ as the superposition principle is not valid and the photocurrent is voltage dependent, which manifests in moderate to low fill factors [68]. However, determining $J_{ph}(V_{oc})$ has its own difficulties [63], so usually the J_{sc} is a decent approximation for the photocurrent density and can be used in equation (4). If the photocurrent density drops by 50% between the J_{sc} and V_{oc}, the resulting error leads to an overestimation of V_{oc}^{rad} by 17.5 mV and consequently overestimates ΔV_{oc}^{nr} and underestimate ΔV_{oc}^{rad}. The higher the fill factor, the less the photocurrent depends on voltage and the lower the resulting error.

Note that for the purpose of calculating V_{oc}^{rad}, the EQE-based equation

$$J_{sc} = q \int_0^\infty EQE \cdot \phi_{AM1.5} dE \tag{6}$$

should be used to calculate J_{sc}; any scaling error in the absolute value of the EQE cancels out with the EQE value appearing in the denominator of equation (4). This holds true even when J_0^{rad} is calculated from the EL since the EL is usually scaled with the help of EQE measurements.

4.3. DB picture of V_{oc} losses

In the DB picture based on Rau's reciprocity theorem [26, 27] the voltage losses are split as follows [7, 29]

$$\Delta V^{DB} = E_g^{PV}/q - V_{oc} = \left(E_{ref}/q - V_{oc}^{SQ}\right) + \left(V_{oc}^{SQ} - V_{oc}^{sc}\right) + \left(V_{oc}^{sc} - V_{oc}^{rad}\right) + \left(V_{oc}^{rad} - V_{oc}\right) \tag{7}$$

$$\Delta V^{DB} = \Delta V_{oc}^{SQ} + \Delta V_{oc}^{Jsc} + \Delta V_{oc}^{rad} + \Delta V_{oc}^{nr} \tag{8}$$

where ΔV_{oc}^{SQ} describes losses compared to the Shockley-Queisser limit [69], ΔV_{oc}^{Jsc} is the loss due to an imperfect J_{sc}, and ΔV_{oc}^{rad} and ΔV_{oc}^{nr} describe radiative and non-radiative losses respectively. A schematic of how the different reference energy levels and voltage losses are related can be seen in figure 2(a). In the following, we qualitatively explain the origins of the different loss terms in equation (8) and how they are determined.

The first loss term $\Delta V_{oc}^{SQ} = E_g^{PV}/q - V_{oc}^{SQ}$ is calculated from the difference between the reference energy (photovoltaic band gap) and the V_{oc} in the Shockley-Queisser limit [7] (calculated with E_g^{PV} as the band gap) and is unavoidable. Even for an ideal solar cell, the V_{oc} is smaller than its band gap due to unavoidable radiative recombination in an absorbing material. This loss ΔV_{oc}^{SQ} is approximately proportional to the reference energy and varies between 0.25 V for $E_g^{PV} = 1.2\ eV$ and 0.3 V for $E_g^{PV} = 2\ eV$.

Next, any reduction in photocurrent density with respect to the short-circuit current density in the Shockley-Queisser limit J_{sc}^{SQ} [7] implies a voltage loss

$$\Delta V_{oc}^{Jsc} = \frac{k_B T}{q} \cdot \ln\left(\frac{J_{sc}^{SQ}}{J_{sc}}\right). \tag{9}$$

The logarithm implies comparably low voltage losses of 17.5 mV for a J_{sc} of 50% of the Shockley-Queisser limit and 5.6 mV at 80% of the Shockley-Queisser limit, with the latter corresponding roughly to the value that today's best OSCs achieve [70]. Reduced photocurrents may result from incomplete absorption or losses in charge carrier collection. The former manifests in a maximum EQE below unity or, often more significantly, a very gradual absorption edge visible on a linear scale of the EQE, both of which can be attributed to the low thickness of optimised OSCs in the absence of light trapping. An inaccurately measured J_{sc}, for example by not performing spectral mismatch correction, induces an error on ΔV_{oc}^{Jsc} that is often negligible in the overall voltage loss analysis; a measurement error of $\pm 10\%$ and $\pm 20\%$ in the J_{sc}

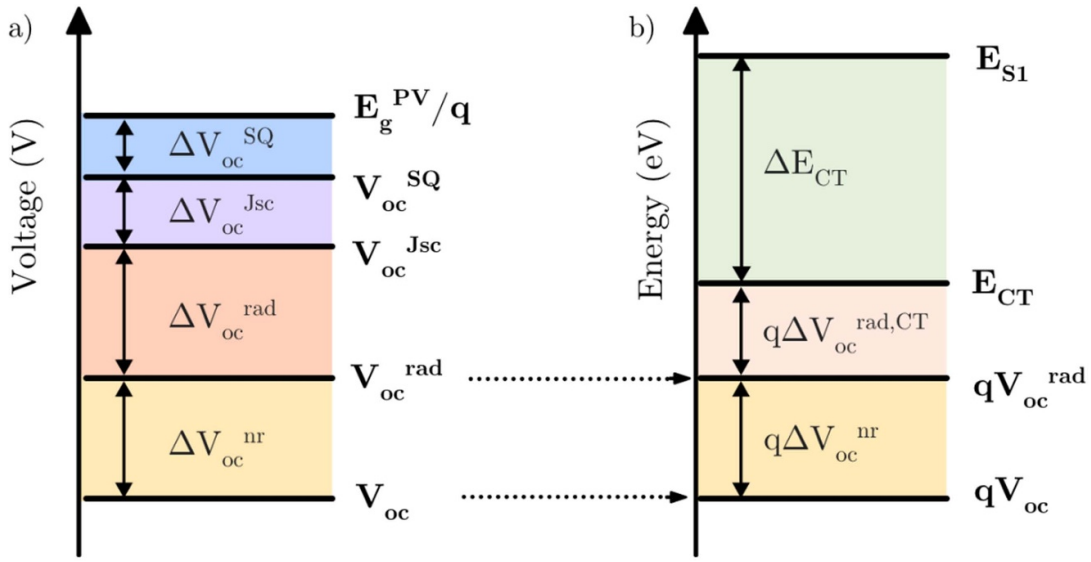

Figure 2. Schematic of the relevant energy levels and voltage losses in (a) the DB picture, and (b) the energetic state picture. In the DB picture, voltage losses are calculated with respect to the 'photovoltaic band gap' (E_g^{PV}). This energy is reduced by ΔV_{oc}^{SQ} to the Shockley-Queisser limit (V_{oc}^{SQ}) defining the theoretical upper limit of V_{oc}. ΔV_{oc}^{Jsc} denotes losses from imperfect short-circuit current density due to non-unity EQE, ΔV_{oc}^{rad} and ΔV_{oc}^{nr} describe radiative and non-radiative losses respectively. In the energetic state picture, the singlet energy E_{S1} is used as a reference energy that is related to the CT state energy E_{CT} by the energetic difference (often called 'driving force') ΔE_{CT}. Radiative losses $\Delta V_{oc}^{rad,CT}$ are defined differently from the DB picture. Non-radiative voltage losses are calculated as the difference between the radiative upper limit (V_{oc}^{rad}) and the measured V_{oc} in both frameworks.

translates to an error of only ~2.5 and ~5 mV respectively in the photocurrent loss, which is likely lower than measurement errors of other steps.

Radiative voltage losses follow directly from the radiative V_{oc}^{rad} calculated in equation (4) as

$$\Delta V_{oc}^{rad} = V_{oc}^{SQ} - V_{oc}^{rad} - \Delta V_{oc}^{Jsc}. \tag{10}$$

The radiative V_{oc}^{rad} decreases, with the corresponding radiative voltage loss ΔV_{oc}^{rad} increasing, for a slowly decaying absorption, or rather EQE, tail. For inorganic solar cells, this is typically caused by (static) energetic disorder resulting in an exponentially decaying 'tail' in the density of states in the sub-gap region. Charge carriers relax into these lower lying states after absorption (and initial thermalization) and subsequently recombine radiatively. This relaxation process presents a loss of energy for the charge carriers. For OSCs, CT states with energies below the singlet are responsible for radiative voltage losses [21] as discussed throughout this review. Depending on the energy and other properties of the CT state, ΔV_{oc}^{rad} can vary from 100s of meV to 10s of meV [71]. Note, that in the Shockley-Queisser limit $V_{oc}^{SQ} = V_{oc}^{rad}$ and $\Delta V_{oc}^{rad} = 0$. Accordingly, for all solar cells, ΔV_{oc}^{rad} must be calculated with respect to V_{oc}^{SQ} and not the band gap. Otherwise, radiative losses are wrongfully inflated by the unavoidable Shockley-Queisser loss term ΔV_{oc}^{SQ} (>250 mV). This might lead to wrong conclusions on what is limiting OSC performance and should be improved.

Finally, non-radiative losses $\Delta V_{oc}^{nr} = V_{oc}^{rad} - V_{oc}$ account for the remaining voltage loss. Since V_{oc}^{rad} and V_{oc} are both robust quantities that can be determined accurately, the same holds true for ΔV_{oc}^{nr}. Non-radiative losses are on the order of 200–500 mV in OSCs [25], with some efficient NFA-based blends achieving losses as low as 150 mV [72]. The exact mechanisms of non-radiative recombination in OSCs are still under discussion but non-radiative recombination is generally understood to involve recombination from the CT state via high-energy phonons of about 150 meV [24, 73]. In principle, trap-assisted Shockley-Read-Hall recombination, the main loss in inorganic solar cells, and surface recombination may contribute to non-radiative losses.

For simplicity or the lack of access to suitable sensitive EQE and EL setups, researchers often only report the total voltage loss $\Delta V = E_{ref} - V_{oc}$. In this case, the reference energy should still be determined accurately using one of the methods recommended above (such as through the inflection point of the EQE). Also, the band-gap dependent Shockley-Queisser losses should be included to account for the variability of the absorption edge in OSC blends. No additional measurements and only relatively simple additional calculations of the V_{oc}^{SQ} [7] are required. We thus recommend reporting $\Delta V = V_{oc}^{SQ}\left(E_g^{PV}\right) - V_{oc}$ as voltage loss whenever EL or EQE with sufficient sensitivity are not accessible.

4.4. Energetic state picture of V_{oc} losses

The energetic state (EN) picture [14] presents the estimation of voltage losses based on the energetic states that are present in OSCs. It relies on the lowest lying singlet energy E_{S1} as reference energy and includes the CT state energy E_{CT} in the loss analysis, highlighting its crucial role in OSC sub-gap absorption and the associated voltage losses. An initial discussion of the determination of E_{S1} was provided in section 4.1, and an in-depth discussion on the correct determination of the CT state energy follows in section 5. In the energetic state picture, voltage losses are defined as

$$\Delta V^{EN} = E_{S1}/q - V_{oc} = (E_{S1} - E_{CT})/q + \left(E_{CT}/q - V_{oc}^{rad}\right) + \left(V_{oc}^{rad} - V_{oc}\right). \tag{11}$$

$$\Delta V^{EN} = \Delta V_{oc}^{CT} + \Delta V_{oc}^{rad,CT} + \Delta V_{oc}^{nr}. \tag{12}$$

Here, V_{oc}^{rad}—and thus ΔV_{oc}^{nr}—are defined as in the DB analysis. Figure 2(b) shows a schematic of the relevant energy levels and voltage losses. It is important to note that radiative losses are coined differently in the two approaches. The DB analysis refers to the difference between the ideal Shockley-Queisser case and the radiative open-circuit voltage (after accounting for losses from photocurrent; $\Delta V_{oc}^{rad} = V_{oc}^{SQ} - V_{oc}^{rad} - \Delta V_{oc}^{Jsc}$) while the energetic state picture refers to the difference between the CT state energy and the radiative open-circuit voltage ($\Delta V_{oc}^{rad,CT} = E_{CT}/q - V_{oc}^{rad}$). ΔV_{oc}^{rad} is generally larger than $\Delta V_{oc}^{rad,CT}$ as it will include some of the loss expressed in ΔV_{oc}^{CT}. Both expressions ΔV_{oc}^{rad} and $\Delta V_{oc}^{rad,CT}$ are referred to as the radiative loss in literature, so care must be taken when comparing results of the different definitions as they cannot be directly related to each other.

ΔE_{CT} highlights the importance of the CT state energy for the V_{oc} of OSCs and is sometimes referred to as the 'driving force' for exciton separation. Its relation to the ionization potential and electron affinity of donor and acceptor molecules in the blends, and the resulting impact for molecular design rules, is still under debate [15, 16]. Reducing ΔE_{CT}, i.e. moving the CT state closer to the donor or acceptor singlet, increases V_{oc}^{rad} and thus decreases ΔV_{oc}^{rad} in the DB picture. Major historic advances in OSC performance, including the success of polymers with lower lying HOMOs and the development of NFAs, are based on reducing ΔE_{CT} (or ΔV_{oc}^{rad} in the DB picture).

While the physics of OSCs are well represented in the energetic state picture by explicitly acknowledging the CT state, it cannot capture some other voltage loss contributions. One example is that the maximum attainable V_{oc} will always be smaller than the reference energy for purely thermodynamic reasons as expressed by ΔV_{oc}^{SQ} in the DB picture. The DB method, on the other hand, does not consider the specific physics of OSCs, which itself has an advantage in that it does not require any fitting of the CT state, a process that comes with its own intricacies as discussed in extensive detail in section 5.

By combining the reciprocity theorem with CT according to Marcus theory (which is discussed in more detail in section 5), Vandewal *et al* derived an expression for V_{oc}^{rad} in terms of CT state properties [21]

$$V_{oc}^{rad} = \frac{E_{CT}}{q} - \underbrace{\frac{k_B T}{q} \cdot \ln\left(\frac{fq2\pi\,(E_{CT} - \lambda)}{J_{sc} h^3 c^2}\right)}_{\Delta V_{oc}^{rad,CT}} \tag{13}$$

where E_{CT} is the CT state energy, f is the oscillator strength of the optical transition between the ground and CT state, and λ describes the reorganization energy of the molecules that form the CT state as they undergo CT . This model predicts an almost linear correlation between V_{oc}^{rad} and E_{CT}/q (with an additional, but negligible $\ln(E_{CT} - \lambda)$ dependence) and thereby motivates the introduction of E_{CT} in the voltage loss account. The model producing equation (13) assumes that all relevant EQE or EL spectral features can be modelled by describing the CT state with Marcus theory. Given the steep decay of the black-body spectrum in equation (3) towards high energies, it is reasonable to assume that only the CT state, and not singlet, absorption affects V_{oc}^{rad}. However, Marcus theory does not account for other effects such as static disorder or energetic hybridization between states. Given how prevalent CT states are in investigating the causes of voltage losses in OSCs, this motivates an in-depth discussion on the accurate analysis of CT state properties.

5. CT state fitting

As discussed in the previous sections, an accurate determination of CT states is not only important for voltage loss analyses, but ultimately paramount for investigating the fundamental operating principles of OSCs and finding ways to further improve their efficiencies. In the following sections, we provide an

in-depth overview of different models applied to describe CT in OSCs. Our aim is to provide a clear overview of the underlying assumptions of each CT model, as well as a guide for when each model is most applicable.

5.1. Marcus theory

5.1.1. CT processes

Marcus theory was originally developed for chemical reactions in solution but has since been applied to other areas of chemistry and physics to describe CT processes from an electron donor (D) to an electron acceptor (A) [74–76]. With this, Marcus theory has proven useful to describe CT processes between organic semiconductors in thin films. Marcus theory relies on the Franck-Condon principle which states that CT is faster than the motion of a nucleus and that electronic transitions generally occur between vibrational energy states that show wave function overlap. In addition, it assumes energy conservation during the CT process. These assumptions have clear implications on how CT between an initial state and a final state is understood to proceed, which we further discuss below.

From thermodynamic principles, we know that the Gibbs free energy (G) of a system depends on the internal energy (U), the pressure (P), volume (V), Temperature (T), and entropy (S) according to

$$G = U + PV - TS. \tag{14}$$

To describe the change in Gibbs free energy (ΔG) upon CT from an initial state to a final state, the CT process is assumed to be isobaric and that changes in the entropic term can be neglected. As a result, the Gibbs free energy is directly related to the internal energy U. The internal energy can further be approximated as the potential energy of the system. In most cases, organic semiconducting molecules and their atomic bonds are modelled as simple harmonic oscillators. This allows to express the potential energy has having a parabolic dependence on the reaction coordinate, a generalized quantity that describes the position, as well as the translational and vibrational movement of all atomic nuclei in the system.

Figure 3 shows a schematic of free energy curves of the ground, excited, and CT state. As described above, classical Marcus theory assumes that transitions between states are isoenergetic (only horizontal transitions on the free energy diagram are allowed), and that CT is faster than the movement of the nuclei (only vertical transitions are allowed). The only place where both conditions are met is at the intersection points of the free energy parabolas, marked by red circles in figure 3.

For a localized exciton to undergo CT from the lowest vibronic excited state (D^*/A) to the CT state (D^+/A^-), an energetic barrier (ΔG^*) between the free energy curves needs to be overcome. Note that the same logic applies for electron or hole transfer if donor or acceptor molecules are excited. Upon CT, the free energy of the system is lowered, and the reaction coordinate is changed, resulting in molecular reorganization realized through a deformation in the molecule or a change of atomic positions, bond lengths or angles. Marcus derived the height of the potential energy barrier, corresponding to the energetic difference between the minimum energy of the CT state and the intersection point of the excited and CT state parabolas, as

$$\Delta G^* = \frac{(\Delta G_0 + \lambda)^2}{4\lambda} \tag{15}$$

where ΔG_0 describes the energetic difference between the minima of the free energy curves of the initial and final state, and λ describes the reorganization energy. The reorganization energy is determined as the excess energy of one state at the minimum energy nuclear coordinate of another state.

We would like to note that Marcus theory is generally discussed in the context of CT from the excited state to the CT state. For simplicity, figure 3 also visualizes this transition. However, when measuring absorption or emission of the CT state, we are usually interested in the direct transition between the ground and CT state. In this case, the same logic applies, but ΔG_0 now needs to be expressed as the energetic difference between the ground and CT state, and λ needs to be correctly assigned to the molecular reorganization of this specific transition.

5.1.2. Marcus theory transition rates

According to Boltzmann statistics, the transition rate of a reaction with an activation energy ΔG from an initial state i to a final state j is proportional to

$$k_{i\to j} \propto e^{\left(-\frac{\Delta G}{k_B T}\right)} \tag{16}$$

where $k_B$is the Boltzmann constant, and T is the temperature. Fermi's golden rule describes the transition rate between the initial and final state as

$$k_{i\to j} = \frac{2\pi}{\hbar} \left|\langle \Psi_j | H | \Psi_i \rangle\right|^2 \rho \tag{17}$$

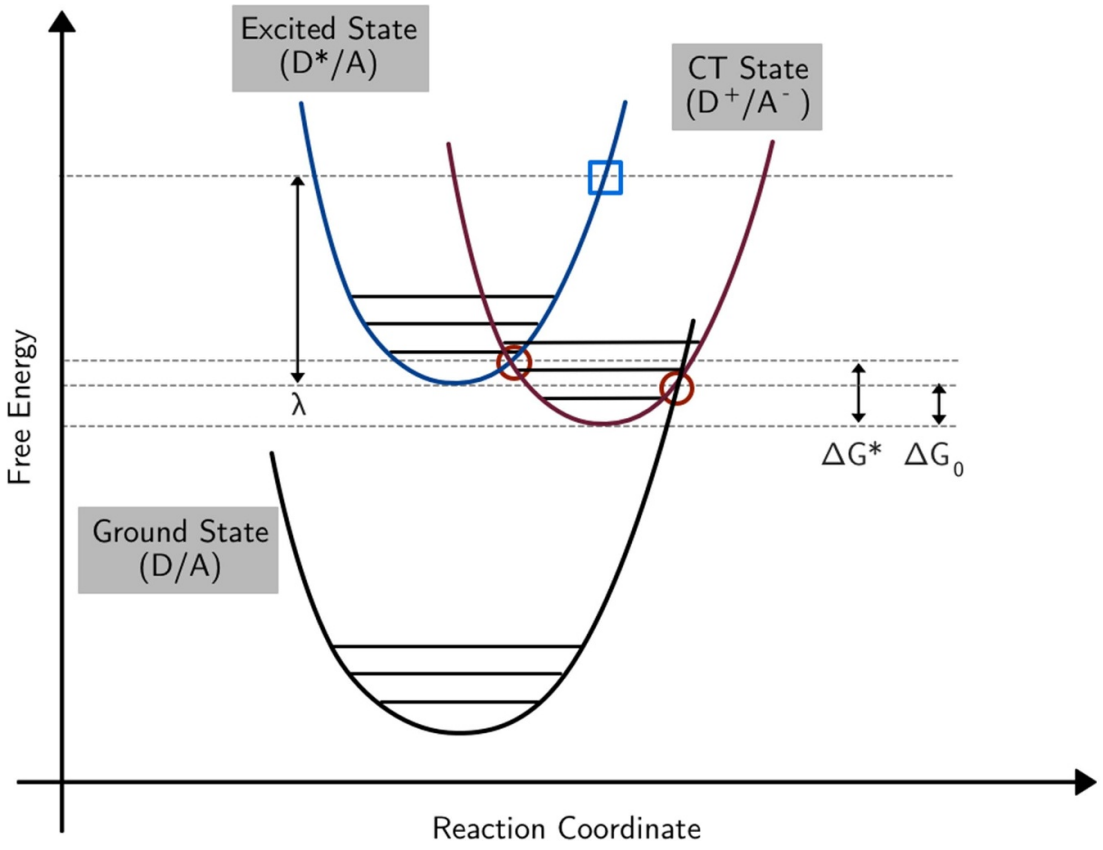

Figure 3. Schematic of parabolic free energy curves of the ground, excited and CT state as a function of the reaction coordinate Q. The reaction coordinate is a generalized quantity that describes the position, and translational and vibrational movement of the atomic nucleus. The horizontal lines indicate vibrational energy states, whose quantized nature is, however, only accounted for in an extension of the Marcus model. The potential energy barrier between the excited and the CT state is given by ΔG^*, and the difference between the minima of the free energy curves is given by ΔG_0. For clearer illustration, the figure shows CT from the excited state to the CT state, however, the same logic applies to direct transitions between the ground and CT state, which are the focus of this review. The reorganization energy λ describes the amount of energy a molecule can minimize by undergoing CT and molecular reorganization. The reorganization energy is determined as the difference in free energy between the initial state at the reaction coordinate of its energetic minimum, and the free energy the system would have if it was still in the initial state, but at the reaction coordinate of the energetic minimum of the final state (highlighted as blue square). The red circles show the intersection points between the free energy curves of the excited and CT state (left) and the ground and CT state (right) where isoenergetic transitions at the same reaction coordinate are possible. Reprinted with permission from [77]. Copyright (2010) American Chemical Society.

where $\Psi_{i,j}$ describes the eigenstates of the initial and final state, H is the Hamiltonian describing the interaction between states, and ρ is the density of final states. The matrix element of perturbation $\langle \Psi_j | H | \Psi_i \rangle$ can be separated into electronic and vibrational contributions, dependent on the electronic coupling term (I_{ij}), and the Frank-Condon factor (FC) describing the vibrational transition.

$$k_{i\to j} = \frac{2\pi}{\hbar} |I_{ij}|^2 \cdot FC. \tag{18}$$

In addition, we can relate equation (16) to the density of final states and connect the height of the potential energy barrier, as derived in Marcus theory, to the activation energy of the transition. This allows us to obtain an equation relating the transition rate to the reorganization energy and the energetic difference between an initial and final state, as has been derived in more detail in [78, 79].

$$k_{i\to j} = \frac{|I_{ij}|^2}{\hbar} \sqrt{\frac{\pi}{\lambda k_B T}}\, e^{\left(-\frac{(\Delta G_0+\lambda)^2}{4\lambda k_B T}\right)}, \tag{19}$$

with

$$FC = \frac{1}{\sqrt{4\pi\lambda k_B T}}\, e^{\left(-\frac{(\Delta G_0+\lambda)^2}{4\lambda k_B T}\right)}. \tag{20}$$

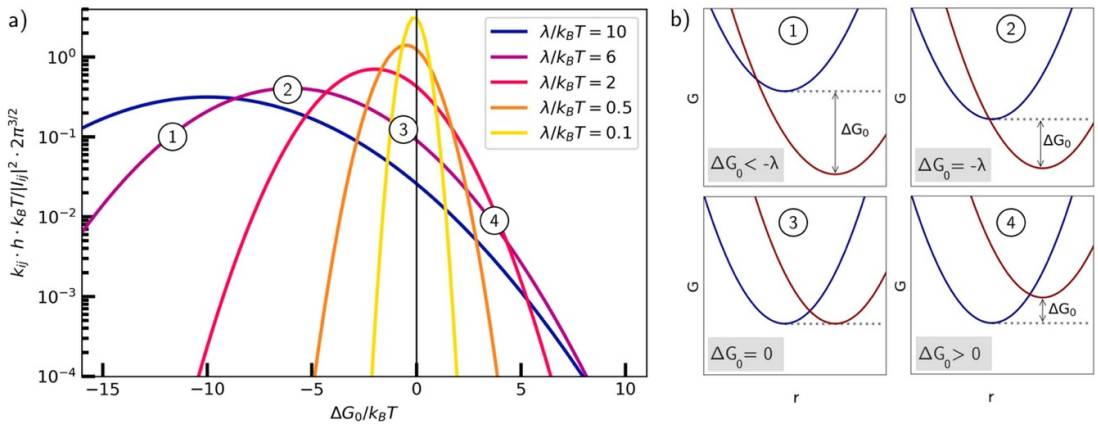

Figure 4. (a) Transition rates as a function of energetic offset ΔG_0 between the relaxed initial and final state as a function of reorganization energy. Note that the transition rates are primarily important for describing thermally activated CT and exciton dissociation processes. The rate is reduced for uphill processes ($\Delta G_0 > 0$) and in the Marcus inverted regime ($\Delta G_0 < -\lambda$). (b) Schematics of potential energy curves of initial states (blue) and final states (red) for different energetic offsets. Case 1 describes the Marcus inverted regime. Case 2 describes a system where the reorganization energy is of the same magnitude as the energetic offset, leading to the most efficient CT . Case 3 describes a system without energetic offset between the initial and final state, and case 4 describes an energetic uphill process. An example of where the four cases might occur on the transfer rate vs. energetic offset curves is shown in (a). Reprinted by permission from Springer Nature Customer Service Centre GmbH: [Springer] [Organic Solar Cells] [78] (2014).

Equation (19) assumes that the thermal energy is significantly larger than the phonon energy ($k_BT \gg \hbar\omega$), meaning that the quantum nature of phonons (or molecular vibrations) does not need to be considered explicitly [80]. Even though it has been argued that this assumption is usually satisfied above 100 K for molecules typically used in OSCs [81], other accounts [80–82] suggest that the quantum nature of phonons needs to be accounted for explicitly.

Figure 4 shows calculations of the transition rate as a function of the energetic offset (ΔG_0) and the reorganization energy (λ) following Marcus theory (equation (19)). Note that this discussion is primarily focused on thermally activated transitions that are relevant for CT and exciton dissociation processes, rather than the direct absorption/emission of CT states. As intuitively expected, if the final state has a higher relaxed energy than the initial state ($\Delta G_0 > 0$, panel 4 figure 4(b)) the transition rate severely decreases. Surprisingly, Marcus theory predicts that the same applies to systems with very large energetic offsets ($\Delta G_0 \ll 0$, panel 1 in figure 4(b)), which is a direct result of the requirement of an isoenergetic CT process. This regime where the transition rate decreases with increasing energetic offset is called the Marcus inverted region (MIR) [74–76, 83, 84]. The reason for the decreasing transition rate is the fact that transitions need to occur at a reaction coordinate smaller than the equilibrium coordinate for both the initial and final state. The MIR has been challenging to verify experimentally [85], though recent work showed the impact of the interfacial driving force on CT processes in thin-film polymer blends [81, 86], quantified the reorganization energy for photoinduced electron transfer in the MIR of a carbon nanotube heterojunction [87], and investigated charge transport in transistors based on thin film small molecules [85] and molecular junctions based on self-assembled monolayers [88]. The highest transition rate occurs for systems where $\Delta G_0 = \lambda$ (case 3 in figure 4(b)) and the potential energy parabolas of the states intersect at the equilibrium reaction coordinate of the initial state. Larger reorganization energies reduce the differential dependence on the activation energy.

5.1.3. Determination of the CT state energy

CT states between an electron donor and electron acceptor were shown to be the lowest energy absorbing and emitting state in an organic semiconductor blend [17, 19–21, 89]. This implies that absorption and emission can occur directly between the ground state and the CT state. With this ΔG_0 in equation (15) is dependent on the energy of the CT state. According to Vandewal *et al* the absorption cross-section (σ_{CT}) can be described by Marcus theory as

$$\sigma_{CT}(E)\,E = \frac{f_{CT}}{\sqrt{4\pi\lambda_{CT}k_BT}} e^{\left(-\frac{(E_{CT}+\lambda_{CT}-E)^2}{4\lambda_{CT}k_BT}\right)} \tag{21}$$

where E_{CT} is the CT state energy, λ_{CT} is the reorganization energy between the ground and CT state, capturing broadening from both intra- and intermolecular vibrations of the complex, f_{CT} is the oscillator strength describing the optical dipole coupling between the two states, and E is the photon energy. As briefly

discussed earlier, the reorganization energy describes the amount of energy the donor-acceptor system can reduce by undergoing CT with corresponding reorganization of the molecular complex. In the final state, a minimum energy is reached for different positional, translational, vibrational, or torsional properties of the molecules. As such, the reorganization energy is more than just a fit parameter, but a fundamental property of the donor-acceptor complex. The reorganization energy between the ground and the CT state is in some cases, e.g. for rigid molecules like C_{60}, similar to the reorganization energy between the excited state and the CT state [81, 90, 91].

If CT states are measured through sensitive absorption techniques, for example through EQE measurements, the CT state absorption cross-section needs to be linked to the EQE. The EQE can be expressed as the product of the absorption rate (η_a) and the internal quantum efficiency (*IQE*). Neglecting interference effects (the validity of this assumption is discussed in detail later), and assuming weak absorption with well-reflecting back electrodes, the EQE is further approximated as

$$EQE(E) = \eta_a(E)\, IQE(E) \approx 2\alpha(E)\, d \cdot IQE(E) \tag{22}$$

where d is the absorber layer thickness, and α is the absorption coefficient [21]. The absorption coefficient in the region of CT absorption equals the product of the absorption cross-section and the number of CT complexes $\sigma_{CT}N_{CT}$. With this, the EQE can be expressed as

$$EQE(E) = \frac{f}{E\sqrt{4\lambda_{CT}k_BT}} e^{\left(-\frac{(E_{CT}+\lambda_{CT}-E)^2}{4\lambda_{CT}k_BT}\right)}, \tag{23}$$

$$f = 2d\eta_a N_{CT} f_{CT} \tag{24}$$

with f as an absorption pre-factor that is dependent on the oscillator strength.

Assuming reciprocity between absorption and emission [27, 28, 55], a similar expression can be derived to describe the EL

$$EL(E) = \frac{E \cdot f'}{\sqrt{4\lambda_{CT}k_BT}} e^{\left(-\frac{(E_{CT}-\lambda_{CT}-E)^2}{4\lambda_{CT}k_BT}\right)}. \tag{25}$$

If the CT state energy is clearly resolvable in the EQE, equation (23) can be used to fit a Gaussian shape to the low energy tail to determine the CT state energy, reorganization energy, and absorption pre-factor. Similarly, EL spectra can be fit with equation (25). In an alternative approach, EL and EQE measurements are combined to determine the CT state energy. For this, the EQE and EL spectra first need to be reduced to remove the dependence on energy in the exponential pre-factor.

$$EQE(E) \cdot E = EQE_R(E) = \frac{f}{\sqrt{4\lambda_{CT}k_BT}} e^{\left(-\frac{(E_{CT}+\lambda_{CT}-E)^2}{4\lambda_{CT}k_BT}\right)}, \tag{26}$$

$$\frac{EL(E)}{E} = EL_R(E) = \frac{f'}{\sqrt{4\lambda_{CT}k_BT}} e^{\left(-\frac{(E_{CT}-\lambda_{CT}-E)^2}{4\lambda_{CT}k_BT}\right)}. \tag{27}$$

The EL spectrum can then be aligned to the same height as the (absolute) EQE spectrum such that $f = f'$ and the CT state energy is determined from the intersection point between the EL and EQE fits [21].

5.1.4. Static and dynamic disorder in the classical Marcus picture

Classical Marcus theory as discussed up until this point describes absorption and emission of a single absorber with a single value for E_{CT} and models the observed vibrational broadening in terms of the reorganization energy [92]. However, disordered films like the photovoltaic active layers of OSCs are not expected to show one single CT state energy. Instead, the statistical spread of how molecules in a disordered thin film pack and arrange leads to microstructural disorder at the interface between donor and acceptor molecules. This microstructural disorder translates into interfacial energetic disorder and an inhomogeneously broadened distribution of CT states [82, 92–94]. Inhomogeneous broadening in this case refers to the fact that different interfaces between donor and acceptor molecules in a disordered thin film might show different interfacial CT state energies but that the collection of all CT state energies is Gaussian distributed. Further evidence for the existence of a distribution of CT states comes from the fact that

equations (23) and (25) predict a strong spectral narrowing at decreasing temperature which has not been observed experimentally.

Burke *et al* first attempted to describe the impact of microstructural and energetic disorder by disentangling dynamic (i.e. temperature dependent) and static (i.e. temperature independent) contributions [92]. They showed that equations (23) and (25) can be used to model CT state absorption and emission if the experimentally determined CT state energy E_{CT}^{exp} and reorganization energy λ_{CT}^{exp} are understood to already incorporate static and dynamic disorder contributions according to

$$E_{CT}^{exp} = E_{CT} - \frac{\sigma_{CT}^2}{2k_BT}, \tag{28}$$

$$\lambda_{CT}^{exp} = \lambda_{CT} + \frac{\sigma_{CT}^2}{2k_BT} \tag{29}$$

where σ_{CT} describes the static disorder, and $2k_BT$ reflects the dynamic disorder of a system [92].

However, the possible impact of static disorder on spectral broadening and device performance is still heavily debated in literature and likely depends on the material system under investigation. Burke *et al* showed that static disorder contributions between 60 and 100 meV adequately describe their studied selection of polymer:PCBM solar cells, a result that has also been confirmed elsewhere [82]. In comparison, other studies [93–95] argue that the impact of static disorder is insignificant. A detailed discussion on alternative sources of spectral broadening follows later after we introduce extensions to the classical Marcus picture. Nonetheless, equations (28) and (29) highlight the difficulty to correctly separate experimentally measured quantities from fundamental properties of energetic states in disordered thin films. For the following equations presented in this review, if disorder is not explicitly included, it is assumed that E_{CT} and λ_{CT} refer to the experimentally determined values that incorporate disorder contributions.

As a side note, measuring the V_{oc} as function of temperature is, in principle, an alternative way of obtaining the CT state energy [21]. The low temperature measurements are extrapolated to 0 K where they coincide with the CT state energy at 0 K. Since the extrapolated value is independent of light intensity [21] using incident light at 1 sun intensity is not a strict requirement. To determine the CT state energy at room temperature, the energetic distribution of CT states, meaning the degree of static disorder, must be known [92] as explained above. Temperature-dependent V_{oc} measurements may thus help to confirm results from fitting room temperature EQE and EL spectra rather than providing a fully independent and accurate determination of E_{CT}.

5.1.5. Limitations of standard Marcus theory to fit CT states

5.1.5.1. Interference effects

One of the assumptions that led to the derivation of equations (23) and (25) to fit CT state absorption and emission from EQE and EL spectra with a Gaussian line shape is that inferences effects in the thin active layers of OSCs can be neglected. This, however, is not guaranteed to be a true assumption. The influence of microcavity effects and out-coupling efficiency on the emission spectrum of organic LEDs has been documented in detail [96–101]. In the context of OSCs, optical simulations are commonly used to understand interference effects and tune device stacks to improve in-coupling of incident light for increased charge generation [52, 102, 103]. In addition, microcavities have been used to further increase device performances by enhancing the EQE [104–108]. In fact, microcavities have been designed to specifically enhance CT state absorption to realize organic infrared photodetectors with improved sensitivity [109, 110].

According to List *et al* [111], most optical studies of OSCs focus on optimizing donor and acceptor molecule absorption and thus increasing the EQE, but little work has been done to understand the corresponding effect of microcavities on emission spectra of CT state emission. In [111], the authors fabricated a range of OSCs, changing the reflective electrodes and varying active layer thicknesses, to show that interference effects play a significant role in determining the spectral shape of the EL. Without correction, applying equation (25) to fit the relevant CT state parameters leads in most circumstances to incorrect results.

Building on the work by List *et al*, Armin *et al* investigated the effects of interference on both the low energy tail of the EQE, the high energy tail of the EL, and the intersection between the two [62]. Their work confirmed that interference effects influence both the spectral shape of the emission spectrum and the measured EQE. The determination of E_{CT}, λ_{CT}, and the absorption pre-factor f therefore lead to different results, depending on whether the EQE or the EL were fit. These discrepancies arise from the fact that EL and EQE are device or 'external' quantities, while CT state properties are material or 'internal' quantities. Simple models that relate the two are not always appropriate. The results of Armin *et al* do not challenge the validity

of the DB principle in general, but they highlight that interference effects break reciprocity in their studied systems as mode coupling and microcavities are experienced differently in emission and absorption processes [62].

The authors further showed that EL spectra are more severely affected by interference effects since microcavities can lead to multi-modality (multiple peaks) in the spectra. Regardless, to increase the accuracy of CT state fitting, it was suggested that emission and absorption spectra are corrected for interference effects. A process to correct EL spectra was presented in [111], and by making this (or similar) code publicly available, the wide-spread implementation of such corrections and improvements in the reliability of fitting EL data would be aided.

To correct the EQE, knowledge of the absorption coefficient of the active layer blend is required. This is a straightforward task above the optical gap, where the complex reflective index can be determined using transmission and reflection spectrophotometry or spectroscopic ellipsometry [112]. Since absorption in the sub-gap region is orders of magnitude lower than above the optical gap, precise measurements of the complex refractive index below the optical gap are very challenging. Reference [62] draws upon the work of Kaiser *et al* to correctly determine the absorption coefficient in the sub-gap region. In their presented approach, the authors used measurements of the complex refractive index to model the absorption above the optical gap using a conventional transfer matrix approach. The results were subsequently combined with highly sensitive sub-gap EQE measurements to determine optical constants in that region [112]. Their code to perform these numerical calculations is publicly available to use in the Supplementary Materials of [112].

As expected, interference effects are strongly dependent on the device architecture and active layer thicknesses. Armin *et al* further showed that the fit results of uncorrected EQE spectra only match those of corrected absorption spectra when active layer thickness are thin (i.e. ≈100 nm) [62]. This might be good news for evaporated small molecule OSCs, where active layer thicknesses rarely exceed 100 nm, but further highlights the need to correct for interference effects when active layers are thicker, as is the case for many solution-processed polymer solar cells.

5.1.5.2. Aligning EQE and EL spectra to characterize low-offset systems

In cases where the CT state is not spectrally resolved in EQE measurements [113–115], the standard approach of EQE fitting may be inadequate. This is the case for systems with low energetic offset between CT and singlet states [116–118], most of which are based on NFAs [113–115, 119, 120], though a few examples of low energetic offsets have also been reported for donor:fullerene systems [14, 121]. Systems that do not show distinct sub-gap absorption features, such as a clear shoulder, are generally assumed to qualify as being 'low-offset' or 'low driving force', meaning that CT and singlet states are close in energy.

To determine the CT state energy of low-offset systems, it has been suggested to combine absorption and emission measurements [14, 21] and take E_{CT} as the intersection point of the reduced EQE and EL spectra (equations (26) and (27)). As discussed in the previous section, this requires that interference effects do not obstruct the use of EL data for CT fitting, and that reciprocity between EL and EQE measurements is given. The critical point in determining the intersection point is to align the height of absorption and emission spectra. For cases where CT state absorption is clearly resolved in an EQE spectrum, the EL is aligned to match the height of the (fitted) CT state peak in the EQE (e.g. figure 3(b)) in [14]). Without a clearly defined CT state peak, consistently aligning the EL to the height of the CT state absorption becomes substantially more challenging. Often, the EL is aligned to the first resolvable peak in the absorption spectrum (e.g. figure 3(e)) in [14]), even if it cannot be assigned clearly to the CT state.

In the following, we demonstrate why this approach is insufficient, possibly leading to >50 meV errors of E_{CT}. In addition to assuming that a lack of sub-gap absorption features arises from a low energetic offset between CT and singlet states, aligning EL spectra to the first strongly absorbing peak implies that the oscillator strength of the $S_0 \rightarrow CT$ state transition is similar to that of the $S_0 \rightarrow S_1$ transition. However, it is generally agreed that direct transitions into the CT state are substantially weaker than transitions between the ground and singlet states [14, 21, 31].

Figure 5 shows schematics of simulated EQE spectra and EL spectra modelled with varying CT state properties. The CT (red dashed lines) and singlet state absorption behaviour (orange solid line) were modelled as Gaussians according to standard Marcus theory and using equation (26). Grey solid lines show the sum of CT and singlet state absorption contributions, assuming that the two transitions can be treated independently. In an EQE experiment, this sum would be measured. The blue dotted lines show emission spectra from the CT state modelled with the same CT state parameters and using equation (27). All modelling parameters were chosen such that the CT state Gaussian is not resolvable from the S_1 peak.

Figure 5(a) shows the effect of varying the absorption pre-factor f in equation (26), which, assuming λ and E_{CT} stay constant, can be directly equated to changes in the CT state oscillator strength f_{CT}. On the other hand, figure 5(b) shows the effect of increasing the CT state energy and reducing the energetic gap between

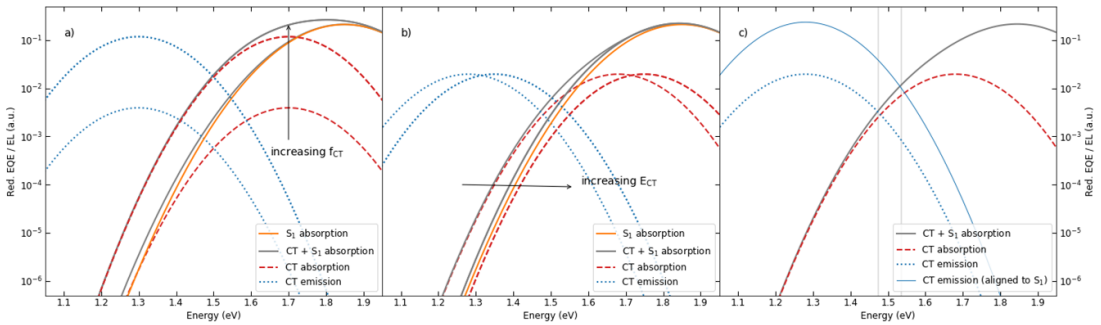

Figure 5. Schematics of simulated EQE and EL spectra for varying CT state properties in the Marcus model. The CT state (red dashed lines) and S_1 (orange solid line) absorption was modelled as Gaussians according to equation (26). The grey solid lines show the sum, that would be measured experimentally, of the CT and singlet state absorption contributions. The blue dotted lines show emission spectra that were modelled with the same CT parameters and using equation (27). All modelling parameters were chosen such that the CT state Gaussian is not resolvable from the S_1 peak in the sum of the spectra as is the case for low-driving force systems. (a) The CT state oscillator strength was increased from 0.001 to 0.03 eV^2 with $E_{S1} = 1.6$ eV, $E_{CT} = 1.5$ eV, $\lambda_{CT} = 0.200$ eV. (b) The CT state energy was increased from 1.48 to 1.55 eV, with $E_{S1} = 1.6$ eV, $f_{CT} = 0.005$ eV^2, $\lambda_{CT} = 0.200$ eV. (c) an example of how aligning the EL to the height of the S_1 peak leads to an intersection point that is higher in energy (right vertical line) than if the EL is aligned to the correct height of the CT state absorption peak (left vertical line).

the CT and singlet state. The exact modelling parameters are reported in the figure caption. These examples show that various parametrizations of CT and singlet state yield similar EQE spectra, where no clear CT state shoulder is visible. It is thus not appropriate to simply assume that the CT oscillator strength is equal to the singlet oscillator strength whenever no clear CT shoulder is visible.

Importantly, for the intersection point to recover the value of E_{CT} that was used to model the EQE and EL, the height of the emission peak needs to match that of the CT absorption, which is lower than the absorption of the singlet and the sum. If the emission spectra are instead aligned to match the first resolvable peak (i.e. the sum absorption peak dominated by the singlet), the extracted CT state energy may carry a very large error. In the example in figure 5(c), an error of 50 meV amounts in the correct determination of the intersection point. When the alignment of the EL is done correctly, the intersection point of the EL with the (fitted) CT state absorption must be considered rather than the full EQE that would be determined in an experiment, since the latter also contains contributions from absorption of the singlet state.

5.1.6. Extending Marcus theory to fit CT and singlet states in EQE data

To increase the accuracy of CT state fitting, the EQE resulting from Marcus theory in equation (23) can be applied to describe not only the CT state, but also the S_1 absorption peak in absorption spectra [122, 123]. Equation (23) is then adapted as

$$EQE_{S1}(E) = \frac{f_{S1}}{E\sqrt{4\lambda_{S1}k_BT}} e^{\left(-\frac{(E_{S1}+\lambda_{S1}-E)^2}{4\lambda_{S1}k_BT}\right)}, \tag{30}$$

where f_{S1} is now related to the density of first excited states, as well as to the strength of the absorption transition between the singlet and the ground state, λ_{S1} is the reorganization energy associated with the transition, and E_{S1} describes the energy of the singlet state [122].

The full EQE spectrum is then given by $EQE = EQE_{CT} + EQE_{S1}$. This assumes that CT and singlet states can be treated independently, and that no hybridization between the states exists. Whether this assumption holds true is dependent on the material system and how closely aligned the CT and singlet state energies are. Without a clearly defined CT state shoulder, some amount of energetic hybridization is likely present, which will be discussed in more detail later. In this case, fitting the singlet and CT state absorption separately would likely lead to an underestimation of the CT state energy and the absorption pre-factor f.

Neglecting hybridization, equation (30) can be used to fit the singlet peak in an EQE spectrum. Here, two different approaches can be applied. Firstly, the S_1 absorption can be fit and subsequently subtracted from the EQE. The remaining tail is then attributed to CT state absorption, as is done in [122, 123]. This assumes that the singlet contribution to the fitted region of the EQE dominates and that CT absorption is negligible, i.e. in the region where the singlet is fit $EQE \approx EQE_{S1}$.

The second approach for incorporating S_1 absorption is to simultaneous fit the sum of two Gaussians describing CT state and singlet absorption. Simultaneous fitting of multiple functions to describe complex spectra is a standard tool in spectroscopic analysis (e.g. [82]). While this approach still considers singlet and

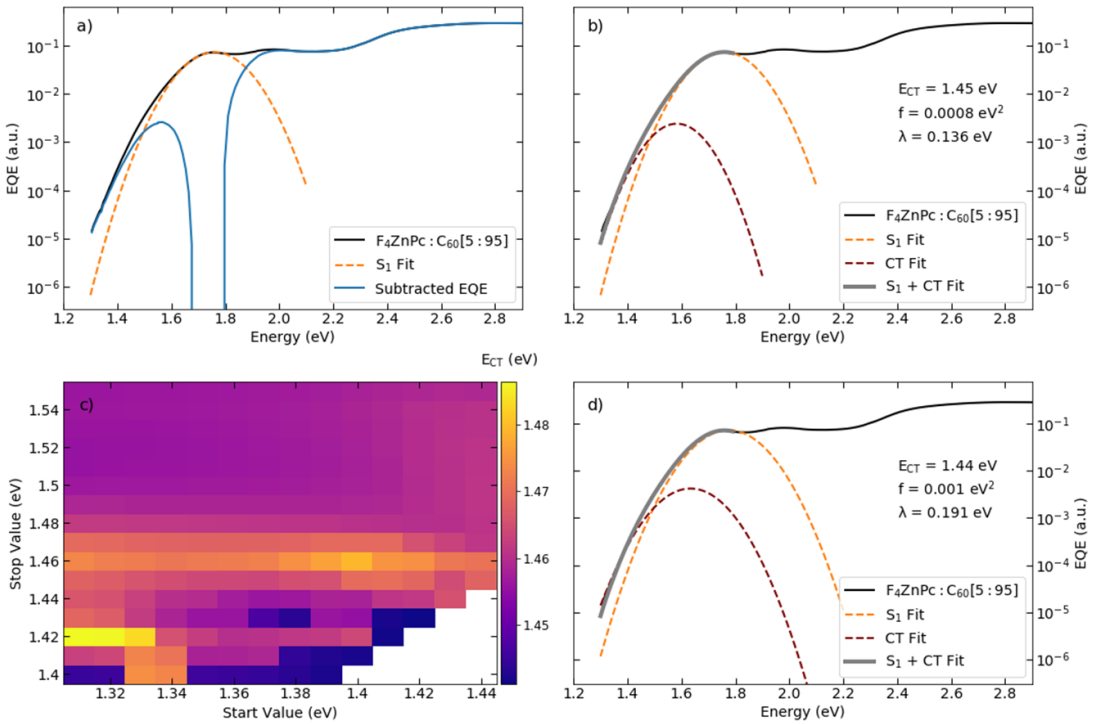

Figure 6. Examples of the two proposed Gaussian fitting approaches, accounting for singlet and CT state absorption, for a system of donor (F_4ZnPc) and acceptor (C60) that does not show clearly resolved sub-gap features. (a) The singlet peak is fit using equation (30) (orange dashed line) and is subsequently subtracted from the data (blue solid line). The remaining sub-gap peak is fit as the CT state. (b) A combination of the singlet (orange dashed) and the CT state (red dashed) fits resulting from (a) are shown. The grey solid line shows the sum of the singlet and CT state absorption contribution. Importantly, CT state fits that respect the overall shape of the tail need to be chosen. (c) By varying the start and stop value of the data range used for fitting, uncertainties of the fit parameters can be calculated. Here, we show an example sensitivity heatmap plot of the CT state energy as a function of start and stop fit values. The area in white shows regions where the model did not converge. (d) Alternatively, rather than fitting the singlet and CT state absorption separately, the two states can be fit simultaneously to the EQE tail as the sum of two Gaussians. The resulting fit values lead to the same CT state energy, but larger absorption pre-factor f and reorganization energy λ than presented using the approach in (b). The fits that are shown in (b) and (d) were chosen as the fits that were achieved with the highest R^2 out of >20 fit ranges.

CT state absorption to occur independently, it reduces the risk of wrongfully attributing CT state absorption to that of the singlet state.

An example comparing these two different approaches is shown in figure 6 for a system without clearly resolvable sub-gap features in the experimental data. Figures 6(a) and (b) show the approach of fitting the singlet absorption peak and subtracting it from the data. After subtraction, a clear Gaussian absorption peak remains in the low-energy region as can be seen in figure 6(a). This absorption peak is fit as the CT state and using equation (23). Importantly, CT state fits should be chosen that respect the overall shape of the EQE tail. The sum of the CT and singlet absorption is shown as a grey line in figure 6(b). Figure 6(d) shows the corresponding results of a simultaneous fitting of the singlet and CT state absorption peak. Both approaches produce a visibly good fit. In comparison to the separate fitting approach, the CT state energy determined through simultaneous fitting is relatively unchanged, but the absorption pre-factor and reorganization energy were found to be larger by 25% and 40% respectively.

To estimate uncertainties of the fits, we recommend the approach presented in [124]. Uncertainties arise from differences in samples and measurements. For a single spectrum, fit values vary depending on what area of the spectrum is fit. Here, a sensitivity analysis is recommended, i.e. to systematically vary the data range and observe changes in the resulting fit parameters. The results can be visualized using heatmaps (as shown in figure 6(c) and used to calculate standard deviations to report as errors on the fit.

In principle, the described best practices allow to fit EQE spectra, even of systems with low offset. The EL spectrum can then be aligned to the height of the fitted CT absorption peak, and the CT energy can be confirmed via the intersection point as described above. Alternatively, the EL scaling factor can be extracted from applying the reciprocity relation and aligning the converted EL data to the EQE tail. The obtained absolute EL spectrum can serve to determine the CT peak in the absorption spectrum, e.g. by fixing or constraining the peak height in the fitting procedure according to its value from EL. However, even with the described methods, CT state analysis might be challenging for low-offset systems [47]. EQE fits may carry

large uncertainty and EL spectra may be influenced by interference. Varying the film thickness, reducing interference by applying a transparent back contact, or including PL and PDS data, as well as advanced optoelectronic modelling of spectra with transfer matrix method and potentially drift-diffusion simulations, may help to quantify parameters with higher accuracy. Finally, it has been suggested that photon emission and absorption in the benchmark low-offset system PM6:Y6 occur from the singlet rather than the CT state, making it impossible to use these measurements to extract information about the CT state, which is supposably still responsible for non-radiative recombination. Similar points will be covered in the context of hybridization in low-offset systems in section 5.3.

5.2. Marcus-Levich-Jortner theory

5.2.1. Phonon modes and transition rates

Whether Marcus theory is fundamentally applicable to describe CT processes in organic semiconductors is still heavily debated in literature [81, 82, 93]. Moving beyond the limitations discussed in the previous paragraphs, several arguments [80] have been brought forward to justify why classical Marcus theory—neglecting any quantum-physical effects—can only describe CT processes of certain material systems to first order if at all. We discuss some of the proposed extensions to Marcus theory in the following sections.

Classical Marcus theory as presented in equation (19) assumes that the energy of internal ($\hbar\omega_i$) and external ($\hbar\omega_e$) vibrational (phonon) modes is substantially smaller than the thermal energy of the surrounding (i.e. $\hbar\omega_i + \hbar\omega_e = \hbar\omega \ll k_BT$) [80]. Under this assumption, thermal energy is sufficient to reach higher vibrational energy states to facilitate CT and the quantum nature of phonons does not need to be considered explicitly. However, it has been argued that in organic thin films, especially in the Marcus inverted regime and at low temperatures, transitions are not just governed by thermal activation but quantum mechanical tunnelling between an initial and a final state becomes significant [81, 125, 126].

Internal phonon modes describe vibrations within one molecule (intramolecular) and are usually indicated as horizontal levels in the potential energy curves of energetic states (refer to figure 3). Intramolecular vibrations are usually on the order of 50–300 meV [82], and often dominated by the high frequency C–C bond vibrations of around 150–180 meV [82, 93, 94, 127, 128]. In comparison, external phonon modes describe intermolecular processes, i.e. vibrations between molecules and their surroundings. External phonon modes are usually classified as low frequency modes and are on the order of 1–10 meV [80, 82, 93, 127].

With this, external phonon modes are smaller than k_BT below around 120 K (where the thermal energy is 10 meV), but internal phonon modes are generally larger than k_BT, rendering the assumption that $\hbar\omega_i \ll k_BT$ untrue. The relative magnitude of intramolecular phonon modes compared to the thermal energy at room temperature suggests that classical Marcus theory falls short in this regime. Therefore, external phonon modes can, in the first instance, be treated classically at room temperature but high frequency internal phonon modes need to be treated quantum mechanically. This led to an extension to equation (19), known as the Marcus-Levich-Jortner (MLJ) equation [80].

$$k_{l\to m} = \frac{|I_{lm}|^2}{\hbar}\sqrt{\frac{\pi}{\lambda_e k_B T}}\sum_{n=0}^{\infty}\frac{e^{-S_i}S_i^n}{n!}\,e^{\left(-\frac{(\Delta G_0+\lambda_e+n\hbar\omega_i)^2}{4\lambda_e k_B T}\right)}. \tag{31}$$

Here, a transition from an initial state l to a final state m is described by the electronic coupling term $|I_{lm}|^2$, the driving force ΔG_0 of the transition (which is $E_{CT} - E$ for descriptions of CT states), and the reorganization energy associated with the external phonon modes (λ_e). In addition, contributions of internal phonon modes are indicated by the subscript i. Equation (31) is, in the first instance, dependent on the dominant high frequency mode with energy $\hbar\omega_i$. This phonon contribution is summed up for all phonon quanta $n = 0 - \infty$. In analogy to equation (20), the quantum-mechanical Franck-Condon weighted density of states is therefore given by

$$FC = \frac{1}{\sqrt{4\pi\lambda_e k_B T}}\sum_{n=0}^{\infty}\frac{e^{-S_i}S_i^n}{n!}\,e^{\left(-\frac{(\Delta G_0+\lambda_e+n\hbar\omega_i)^2}{4\lambda_e k_B T}\right)}. \tag{32}$$

Here, S_i is the so-called Huang-Rhys parameter which is a dimensionless factor that depends on changes in the equilibrium reaction coordinate when a system undergoes a transition from one state to another. The Huang-Rhys parameter depends on the coupling strength of a transition and is related to the reorganization energy λ as

$$S_i = \frac{\Delta Q^2 m\omega_i}{2\hbar} = \frac{\lambda}{\hbar\omega_i} \tag{33}$$

where $\hbar\omega_i$ is the energy associated with vibrational mode i, ΔQ is the change in the equilibrium reaction coordinate (introduced earlier) upon CT, and $m\omega$ is the force constant of the system. For rigid molecules, where the $0-0$ transition is the dominant feature in absorption or emission measurements, the Huang-Rhys factor is on the order of $S \leqslant 1$ [82]. With larger Huang-Rhys factors, the maxima of the $0-0$ transition are eventually no longer resonant, leading to a large Stokes shift between absorption and emission. Low frequency intermolecular modes are generally described by lager Huang-Rhys factors, leading to phonon wings with a Gaussian line shape as discussed in more detail in [82].

Classical Marcus theory as described in equation (19) requires knowledge of the electronic coupling term (and therefore the oscillator strength), which can be fit from spectroscopic data [129] or determined via quantum mechanical calculations [130–132], for example using density functional theory (DFT) approaches [133]. Otherwise, equation (19) is primarily dependent on E_{CT} and λ. In comparison, equation (31) requires knowledge of dominant vibrational modes to determine $\hbar\omega$ and thereby the Huang-Rhys factor S. Experimentally, vibrational modes can be probed via Raman spectroscopy or determined via DFT calculations (e.g. [128]).

5.2.2. CT state energies and disorder in the MLJ picture

Following from equation (31), the MLJ equation can be extended to describe the EQE as

$$EQE(E) = \frac{f}{E\cdot\sqrt{4\lambda_{CT}k_BT}}\sum_{n=0}^{\infty}\frac{e^{-S_i}S_i^n}{n!}e^{\left(-\frac{(E_{CT}+n\hbar\omega_i+\lambda_{CT}-E)^2}{4\lambda_{CT}k_BT}\right)}. \tag{34}$$

Importantly, applying the reciprocity relation, and determining the EL as the product of the EQE and the black-body spectrum, yields an expression for the EL which is no longer mirror symmetric to the EQE, as discussed in detail by Göhler *et al* [93].

$$EL(E) = \frac{E\cdot f'}{\sqrt{4\lambda_{CT}k_BT}}e^{\left(-\frac{E_{CT}}{k_BT}\right)}\sum_{n=0}^{\infty}\frac{e^{-S_i}S_i^n}{n!}e^{\left(-\frac{n\hbar\omega_i}{k_BT}\right)}e^{\left(-\frac{(E_{CT}+n\hbar\omega_i-\lambda_{CT}-E)^2}{4\lambda_{CT}k_BT}\right)}. \tag{35}$$

The positive vibrational contribution ($+n\hbar\omega_i$) in the exponential removes the mirror symmetric behaviour of absorption and emission spectra that was observed in classical Marcus theory. In addition, the emission is now damped by the $e^{\left(-\frac{E_{CT}}{k_BT}\right)}$ and $e^{\left(-\frac{n\hbar\omega_i}{k_BT}\right)}$ pre-factors, as discussed in [93]. The presentation of equation (34) differs from how the MLJ model was presented by Kahle *et al* where the $e^{\left(-\frac{E}{k_BT}\right)}$ factor entering the equation by multiplication with the black-body spectrum was not propagated into the exponential of the absorption spectrum [82]. It is important to note that both Kahle *et al* and Göhler *et al* agree on the form of equations (34) and (35). The broken mirror symmetry is, however, only clearly visible in how Göhler *et al* present the equation.

Following the approach presented by Burke *et al* to separate the contributions of static and dynamic disorder by assuming a Gaussian distributions of CT state energies [92], equations (34) and (35) can be extended to a disordered MLJ model [82, 93].

$$EQE(E) = \frac{f}{E\cdot\sqrt{4\lambda_{CT}k_BT+2\sigma_{CT}^2}}\sum_{n=0}^{\infty}\frac{e^{-S_i}S_i^n}{n!}e^{\left(-\frac{(E_{CT}+n\hbar\omega_i+\lambda_{CT}-E)^2}{4\lambda_{CT}k_BT+2\sigma_{CT}^2}\right)}, \tag{36}$$

$$EL(E) = \frac{E\cdot f'}{\sqrt{4\lambda_{CT}k_BT+2\sigma_{CT}^2}}e^{\left(-\frac{E_{CT}}{k_BT}+\frac{\sigma_{CT}^2}{2(k_BT)^2}\right)}\sum_{n=0}^{\infty}\frac{e^{-S_i}S_i^n}{n!}e^{\left(-\frac{n\hbar\omega_i}{k_BT}\right)}e^{\left(-\frac{\left(E_{CT}+n\hbar\omega_i-\lambda_{CT}-\frac{\sigma_{CT}^2}{k_BT}-E\right)^2}{4\lambda_{CT}k_BT+2\sigma_{CT}^2}\right)}. \tag{37}$$

As before, the broken mirror symmetry between the EL and EQE is apparent.

5.2.3. Multiple phonon modes

As mentioned earlier, the underlying assumption to treat vibrational modes classically is that the energy of the phonon mode is smaller than k_BT. For external phonon modes with energies 1–10 meV [80, 82, 93, 127], this requirement is satisfied at temperatures relevant for the operation of OSCs. However, at low enough temperatures, this simplification breaks down, and external phonon modes need to be considered explicitly as well. This was discussed in detail in the works of Kahle *et al* and Göhler *et al* [82, 93]. The Franck-Condon

weighted density of states is then proportional to the sum over the product of multiple phonon modes and their corresponding vibrational overtones.

$$FC \propto \sum_{m_i} \prod_i \frac{S^{m_1} e^{-S_i}}{m_i!} \,. \tag{38}$$

In the case where only the highest energy intra- and intermolecular modes need to be considered, the EQE and EL now become

$$EQE(E) = \frac{f}{E \cdot \sqrt{4\lambda_{CT} k_B T + 2\sigma_{CT}^2}} \sum_{n=0}^{\infty} \sum_{m=0}^{\infty} \frac{e^{-S_0} S_0^n}{n!} \frac{e^{-S_1} S_1^m}{m!} e^{\left(-\frac{(E_{CT}+n\hbar\omega_0+m\hbar\omega_1+\lambda_{CT}-E)^2}{4\lambda_{CT}k_BT+2\sigma_{CT}^2}\right)}, \tag{39}$$

$$EL(E) = \frac{E \cdot f'}{\sqrt{4\lambda_{CT} k_B T + 2\sigma_{CT}^2}} e^{\left(-\frac{E_{CT}}{k_B T} + \frac{\sigma_{CT}^2}{2(k_B T)^2}\right)} e^{\left(-\frac{n\hbar\omega_0 + m\hbar\omega_1}{k_B T}\right)} \times \sum_{n=0}^{\infty} \sum_{m=0}^{\infty} \frac{e^{-S_0} S_0^n}{n!} \frac{e^{-S_1} S_1^m}{m!} e^{\left(-\frac{\left(E_{CT}+n\hbar\omega_0+m\hbar\omega_1-\lambda_{CT}-\frac{\sigma_{CT}^2}{k_b T}-E\right)^2}{4\lambda_{CT}k_BT+2\sigma_{CT}^2}\right)} \tag{40}$$

where the subscript 0 refers to the intramolecular mode with overtones n, and the subscript 1 refers to the intermolecular mode with overtones m.

5.2.4. Sources of spectral broadening in different models

Having introduced a variety of models that expand on Marcus theory, we now discuss how these models have been applied to explain line-width broadening of absorption or emission spectra. Current understanding in literature is that spectral broadening can be of homogeneous (i.e. affecting all absorbing and emitting molecules the same), or inhomogeneous nature (i.e. affecting different absorbing and emitting molecules differently, but overall leading to a Gaussian line shape to describe the collective absorption or emission of a film) [24]. Static disorder based on a statistical distribution of how molecules pack causes inhomogeneous broadening, while vibrational contributions arising from dynamic disorder are understood to affect all molecules homogeneously [82, 92, 93].

However, a lack of agreement still exists in literature on which mechanisms are dominant contributors to spectral line-width broadening and how it relates to different material properties. Energetic disorder impacts charge carrier generation and recombination mechanisms, therefore directly impacting device parameters like the open-circuit voltage [94]. Similarly, high frequency modes were shown to link to non-radiative recombination [24], and therefore leading to losses in the open-circuit voltage. Understanding the origin of energetic disorder and the impact of vibrational modes are, in our opinion, currently one of the most important research questions in the field of organic photovoltaics. Addressing these research questions will help to estimate performance limits more accurately and understand whether and how dominant loss mechanisms can be overcome. In the following, we discuss the signatures in EQE data characteristic of the different CT models introduced earlier. We then summarize current experimental findings on which physical model is most appropriate for different material systems.

Figure 7 shows a comparison of modelled EQE tails using the CT models discussed in the previous sections. The modelling parameters were chosen to reflect values published in literature for polymer or small molecule OSCs (e.g. [82, 94]) and are listed in the figure caption.

As discussed by Tvingstedt *et al* [94], the classical Marcus model excluding static disorder predicts vanishingly small CT rates and absorption/emission line-widths with decreasing temperatures. This can be clearly observed in figure 7(a). In addition, the Gaussian variance of the spectral line-width is expected to be directly linearly dependent on temperature in the classical Marcus model, which has never been experimentally confirmed [94].

As can be seen in figure 7, the inclusion of static disorder in the model reduces the dependence of the line-width on temperature and leads to spectral broadening. However, the main differences between assuming zero static disorder (figure 7 left column) and a static disorder of 50 meV (figure 7 right column) are only visible at very low temperatures and much less dominant for the other temperatures shown here.

Including a quantum mechanical treatment of vibrational modes, shown in figures 7(c)–(f), removes the mirror symmetry of the spectrum. Without static disorder, the vibrational overtones lead to strong periodic peaks in the high energy region at low temperatures, which have, to the best of our knowledge, not yet been observed experimentally. These peaks are still visible when inter- and intramolecular modes are treated

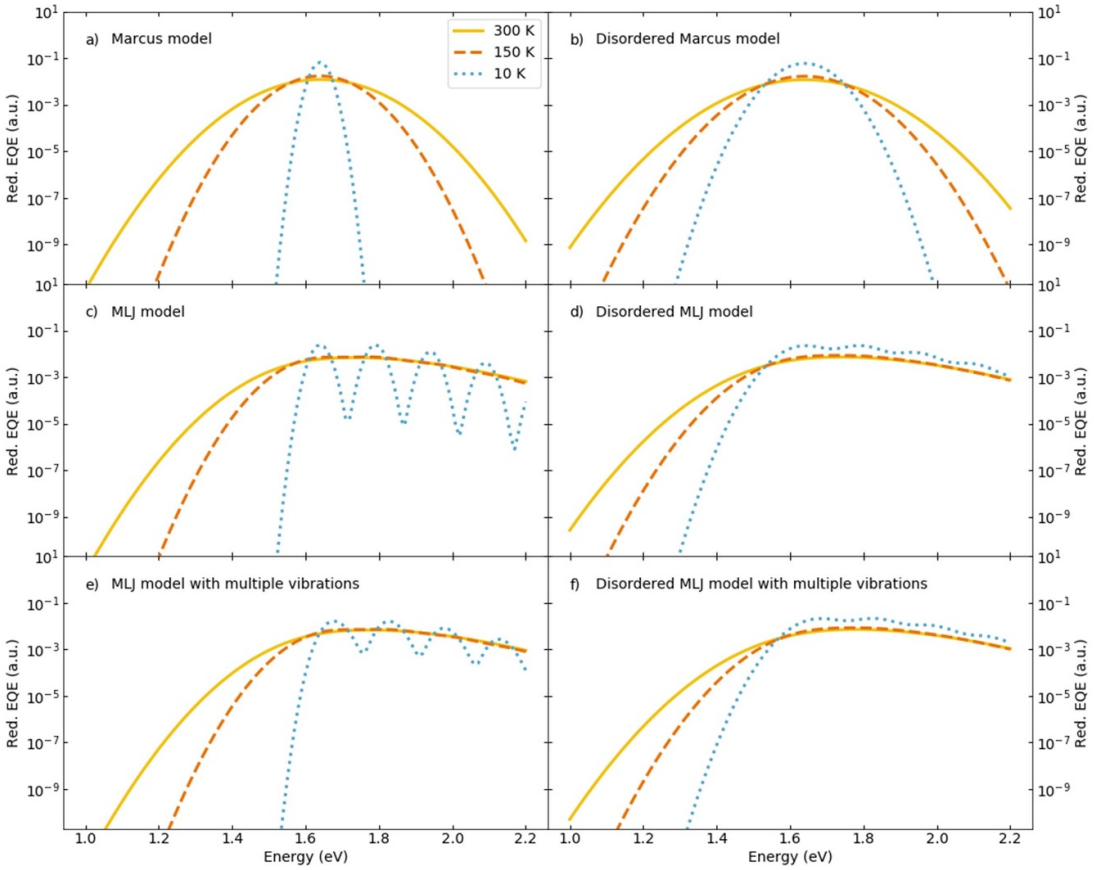

Figure 7. Modelled EQE tails based on different CT models. For clarity, (a) Marcus model refers to equation (23), (b) disordered Marcus model accounts for the explicit consideration of disorder (equations (28) and (29)) in equation (23), (c) MLJ model to equation (34), (d) Disordered MLJ model to equation (36), and (e) and (f) the (Disordered) MLJ model with multiple vibrations stems from equation (39) in the main text. All modelling parameters were chosen as based on values published in literature for polymer or small molecule OSCs: $E_{CT} = 1.45\ eV$, $\lambda_{CT} = 190\ meV$, $f = 0.003\ eV^2$, $\sigma_{CT} = 50\ meV$, $S_i = 1$, $\hbar\omega_i = 150\ meV$, $S_{low} = 4$, $\hbar\omega_{low} = 10\ meV$, where the subscript i describes intramolecular, high frequency vibrations, and the subscript low marks inter-molecular, low frequency vibrations.

quantum mechanically, shown in figure 7(e), though their periodic amplitude is reduced. Including static disorder in either model substantially dampens the impact of the periodic overtones.

Kahle *et al* investigated how well a Franck-Condon fit, including static disorder and a quantum mechanical treatment of high and low frequency modes similar to the discorded MLJ model with multiple vibrations, describes the temperature dependent EQE and PL spectra of an MeLPP:PCBM system [82]. This was compared to applying the Marcus-Levich-Jortner model treating only high frequency modes quantum mechanically. They found that both models describe the system equally well, as long as static disorder is considered [82]. For this system, they found a static disorder of 67 meV to be appropriate, matching previously reported values of 60–100 meV for polymer systems [92].

Tvingstedt *et al* agreed that a Franck-Condon description based on high and low frequency modes is appropriate. However, they did not find experimental evidence in the absorption and emission spectra of their small molecule and polymer solar cells to justify that a substantial contribution to the line-width comes from static disorder [94]. Similar results have also been shown in the theoretical work of Panhans *et al* [134] and the experimental work of Göhler *et al* who argued that the extended Marcus-Levich-Jortner model, introduced in section 5.2.3 and taking low and high frequency vibrations into account but assuming no static disorder, can adequately fit absorption and emission spectra of their dilute small molecule devices [93].

In contrast, the recently published work by Yan *et al* criticised that the material systems studied by Tvingstedt and Göhler *et al*, i.e. dilute donor:fullerene systems, have previously been studied precisely because morphological disorder is minimised [135]. Polymer based solar cells show a range of disorder contributions, e.g. large confirmational and torsional disorder [136], electronic anisotropy, and possible phase aggregation, that are not present in dilute small molecule blends [135]. In multiple accounts, static disorder was found to have a strong impact on extracted CT state parameters and recombination losses for polymer based solar cells [136]. In addition, it was argued that the sphere-like nature of fullerene acceptors promotes distortion and bending of donor molecules, increasing both dynamic and static disorder.

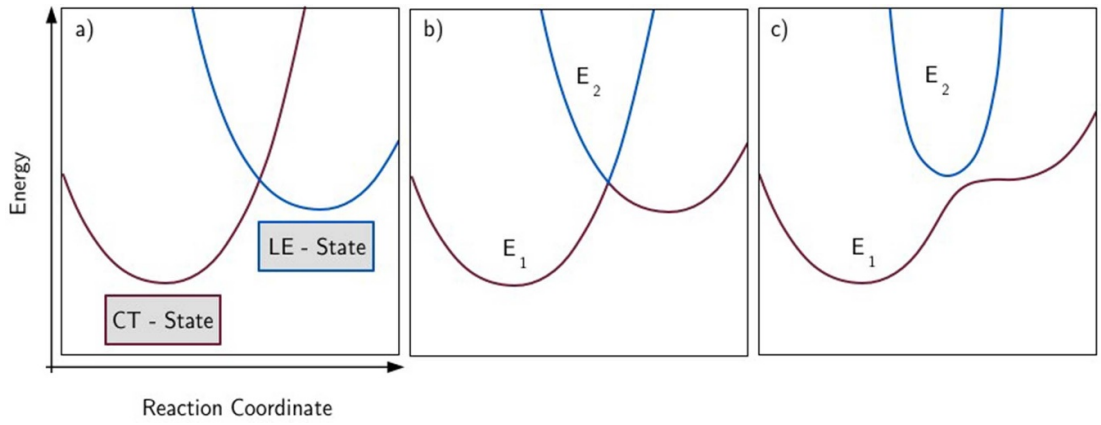

Figure 8. Schematic diagrams of potential energy curves. (a) Diabatic state without hybridization between the CT and LE singlet state. In comparison, adiabatic states with (b) small, and (c) large electronic coupling are characterized by hybridization between the two states. Reprinted by permission from Springer Nature Customer Service Centre GmbH: [Springer] [Organic Solar Cells] [78] (2014).

In comparison, NFAs with rigid backbones cause less disorder [136], which might be another reason for why they work so well in organic solar cells.

In conclusion, future studies of static and dynamic disorder are encouraged to be performed on both small molecule and polymer-based systems. In addition to measuring temperature dependent absorption and emission spectra, experimental and theoretical studies [136] of the interfacial microstructure and phase aggregation are crucial to providing a more complete picture of the possible impact of static disorder on CT state properties [135].

5.3. Three-state models

The CT state models introduced up until this point all assume that emission and absorption transitions occur via two states, i.e. the ground and CT state. However, several recent publications argue for the use of a three-state model accounting not only for coupling between the ground state and CT state, but also incorporating contributions of electronic and vibrational coupling with the singlet (local excited (LE)) state on donor or acceptor molecules when CT and singlet states are close in energy. In the following sections, we introduce the impact of hybridization between states on potential energy curves and discuss a selection of recently published three-state models.

5.3.1. Adiabatic vs diabatic states

Electronic transfer processes can be described via diabatic or adiabatic states [137]. Diabatic states are defined as pristine states without hybridization, while adiabatic states are characterized by hybridization between the ground, singlet, and CT state. Figure 8 shows a schematic of the potential energy curves of diabatic and adiabatic states. In the context of a donor-acceptor interface, a diabatic CT state corresponds to a Coulomb-bound electron–hole pair between the D^+ cation and the A^- anion. A diabatic LE state consist of an exciton fully localized on either the donor or acceptor molecule.

5.3.2. Three-state model for CT state fitting

To the best of our knowledge, the work by Chen *et al* [72, 138], provide currently the most detailed account for extending the three-state model to simulate CT state absorption using advanced computational approaches, and fitting the CT state absorption of experimental data. They introduced a model to account for both the electronic coupling (hybridization) between the ground and CT state, in addition to the coupling between the CT and singlet state (equations (11)–(13) in [138]).

They showed through simulations that the molecular packing at the donor/acceptor interface greatly impacts the spectral shape of CT state absorption, as well as relevant CT state properties. This has been experimentally and theoretically confirmed elsewhere [139–142]. Increased hybridization between the energetic states leads to an increase in the absorption intensity of the CT state, caused by an intensity borrowing mechanism.

Comparing Chen *et al*'s three-state approach to a standard two-state approach shows that a two-state approach consistently overestimates the relaxation energy of the CT state, underestimates the CT state energy, and incorrectly attributes contributions of the singlet absorption to the CT absorption, thereby overestimating the hybridization between the CT and singlet states [138]. They further show that strong

absorption intensities between the CT and singlet absorption peaks can be attributed to 'hot' vibronic CT states caused by the coupling of the CT and singlet state, rather than to higher energy CT states (e.g. CT_2, CT_3 etc) as done in other accounts [143].

Interestingly, when comparing Chen *et al*'s three-state approach to the MLJ model introduced earlier, they find better agreement across their studied systems than if a simple two-state model, not accounting for vibrations, is applied. This suggests that, while a three-state model might describe the physics of organic donor-acceptor systems most accurately, a big improvement in the accuracy of fitting CT states can be achieved by explicitly considering high frequency vibrational modes. Nonetheless, the work of Chen *et al* highlights the need for accessible models accounting for hybridization between electronic states that can be easily implemented across research groups.

6. Discussion of advanced models for characterizing CT states and voltage losses

To finish our discussion of the different CT state models, we comment on the most suitable applications for each approach, as well as the necessary trade-off between physical accuracy and complexity. The simplest and hence most used approach is fitting of a Gaussian function via the classical two-state Marcus model. Yet, as explained in detail in the previous sections, classical Marcus theory has certain shortcomings that might warrant the use of more physically accurate but more complex models.

The first addition to classical Marcus theory is the explicit consideration of static and quantized dynamic disorder. Even though the exact impact of static disorder on the line-width broadening is still debated [93, 94, 135], static disorder is likely more relevant for polymer blends, with the many more torsional and conformational degrees of freedom of the molecules, compared to films based on small molecules.

The need to explicitly consider the quantum nature of vibrational modes arises when the energy of the phonon modes is no longer smaller than the thermal energy ($\hbar\omega_i \ll k_B T$). For high frequency, intramolecular vibrational modes caused by C–C or C–H bond vibrations greater than 100 meV [32, 80, 81] [69–71], as is in principle always the case for organic semiconducting molecules, the semi-classical MLJ model, which considers intramolecular modes quantum mechanically, is the most appropriate.

An experimental challenge of the MLJ model, however, is that instead of fitting three free parameters, as is the case for classical Marcus theory were E_{CT}, λ_{CT}, and f are fit, the vibrational modes ($\hbar\omega_i$) or the Huang-Rhys parameter (S_i) are needed as input to reach a reasonable amount of free parameters in the fit. Some of these parameters can be determined experimentally using Raman spectroscopy, which not every research group has access to, or computationally determined via DFT simulations [128, 133]. An estimation of these parameters based on previously published results should, however, suffice but might introduce small errors across different material systems.

A further explicit consideration of the quantum-mechanical nature of low frequency, intermolecular modes will in most instances not be necessary, unless material systems are compared at very low temperatures (i.e. lower than ~120 K). While studies at these low temperatures would help to deconvolute inter- and intramolecular effects that are convoluted at higher temperatures, they are not required for the simulation of device operating conditions. While DFT calculations can easily determine internal vibrational modes, the complex interactions between individual molecules and surrounding environment are extremely challenging if not impossible to determine computationally. As such, an explicit consideration of both internal and external phonon modes would require the fitting or input of seven parameters (E_{CT}, λ_{CT}, f, $S_0/\hbar\omega_0$, $S_1/\hbar\omega_1$) which might be challenging to implement or overparameterize the data.

The biggest advance of our understanding of different material systems is likely achieved by employing a three-state model over the two-state approach of Marcus or MLJ theory. The three-state approach, which considers energetic hybridization between ground, singlet, and CT state, is not just limited to low energetic offset systems such as those of NFAs. In fact, the three-state model has previously been successfully applied to fullerene-based acceptors [117, 138].

To evaluate how much information can be drawn from applying a three-state approach, donor-acceptor systems need to be classified into three categories: (1) systems with a large energetic offset between the singlet and CT state energies and no hybridization between energy states, (2) systems with a large energetic offset and partial hybridization, and (3) systems with a small energetic offset and partial to strong hybridization. Here, EQE and EL spectra are crucial to estimate which category a material system falls into. The less spectrally resolved the CT state is from the singlet state, the more hybridization will play a role.

However, three-state models are not as easily applicable as fitting simple Gaussian functions to absorption and emission spectra. Rather than fitting one analytical equation, the model presented in literature [72, 117] requires complex numerical evaluations of Hamiltonians and corresponding calculations of the systems eigenstates. Even if the simulation code is made publicly available, the current approach requires specialist knowledge to fit spectra accurately.

The accurate determination of hybridization of energetic states is, however, not only crucial for correct determination of CT state properties but is immensely important for an increased understanding of dominant sources of voltage losses, and whether an intensity borrowing mechanism between different energetic states reduces radiative and non-radiative voltage losses. With the availability of simple and easily accessible three-state approaches, we would be able to gain this experimental understanding across different classes of materials. The next logical step in the further development of three-state models is the inclusion of static disorder and electronic delocalization, which were shown to impact CT absorption [81, 82, 92, 144]. On this point, however, care should be taken to develop models that are physically representative, rather than models with enough free parameters to be able to fit any spectrum with high confidence.

To connect our discussion of an accurate determination of CT state properties back to voltage losses, we refer to equation (13) which connects the radiative upper limit of the open-circuit voltage V_{oc}^{rad} to the CT state properties. Equations like this are extremely useful in the design of novel molecules since they indicate which (inter)molecular properties should be improved to achieve better solar cell performance. For example, the expression in the logarithm of equation (13) is larger than one and predicts a decrease of ΔV_{oc}^{rad} with decreasing oscillator strength of the CT transition. This suggests that it would be a good idea to aim for a low CT oscillator strength to increase V_{oc} and thereby the overall PCE. However, this logic is incomplete since it does not consider the effect of the oscillator strength on non-radiative recombination.

Equation (13) assumes that all relevant EQE or EL spectral features can be modelled using the classical two-state approach as defined via Marcus theory and neglects other effects such as static disorder. As discussed above, it has been argued that MLJ theory or the three-state model better describe recombination from or absorption into the CT state. Benduhn *et al* developed a model applying MLJ theory [24] and yielding a refined expression for V_{oc}^{rad} as well as an expression for non-radiative recombination losses that were found to largely rely on E_{CT}—also known as the energy gap law in organic molecule research.

The reason behind this dependence is a decreased vibrational overlap of the wave functions of the ground and the CT state, reducing non-radiative loss pathways. The model was further refined by Azzouzi *et al* [73], who presented an illustrative overview of how different CT states properties affect V_{oc}^{rad} and ΔV_{oc}^{nr}. For example, they confirmed that an increase in the CT state oscillator strength leads to a decreased V_{oc}^{rad}. Simultaneously, non-radiative recombination increases, thereby keeping the experimentally determined V_{oc} approximately constant. Their model predicts the largest voltage loss improvements with a decreasing reorganization energy, increasing CT state energy, and decreasing energetic gap between singlet and CT state energy.

Eisner *et al* [117] investigated the effect of energetic hybridization, i.e. a three-state model, on radiative and non-radiative voltage losses by studying a range of donor/acceptor blends with varying energy levels, including fullerene and NFAs. They found that for certain blends with moderate to low energetic offset, hybridization between the singlet and CT state becomes significant. With an increasing CT state energy, non-radiative recombination via the CT state is reduced according to the energy gap law [24]. The observed voltage loss trends of systems with low energetic offset could not be explained by changes in E_{CT} alone [117]. Instead, it was suggested that non-radiative recombination in low offset systems is not just determined by the emission properties of the CT state, but also by those of the S_1 [6, 117, 145–148]. Through an intensity borrowing mechanisms, highly luminescent S_1 states can increase the luminescence of the CT state, thereby reducing non-radiative recombination.

This lead Eisner *et al* to define an effective oscillator strength of the ground to CT state transition for systems that show hybridization between energetic states as

$$f^{*}_{CT-S_0} = f_{CT-S_0} + \frac{f_{S_1-S_0} V^2_{S_1-CT}}{\Delta E^2_{CT}} + \frac{(f_{S_1-S_0})^2 (f_{CT-S_0})^2 V_{S_1-CT}}{\Delta E_{CT}}, \tag{41}$$

where f_{CT-S_0} and $f_{S_1-S_0}$ describe the oscillator strength of the ground to CT state or ground to singlet state transitions in the absence of energetic hybridization, and V_{S_1-CT} is the coupling strength between the singlet and CT state. A schematic of the corresponding processes is shown in figure 9. Despite the decreasing non-radiative recombination for low offset systems, Eisner *et al.* confirmed that the total recombination rate increase with higher electronic coupling, suggesting a limit for how far voltage losses in OSCs can be reduced.

Further opportunities for voltage loss improvements are presented, for example, by Panhans *et al* who simulated the impact of electronic and electron-phonon coupling on the absorption line-width and radiative losses of low donor small-molecule OSCs [134]. They expanded the three-state approach and account for hybridization between CT states (CT-CT coupling), and between singlet and CT states (LE-CT coupling). They found that a dominant contribution to voltage losses arises from electron-phonon coupling, like zero-point vibrations that they argue are also present at 0 K. In comparison to Azzouzi *et al* [73], their work

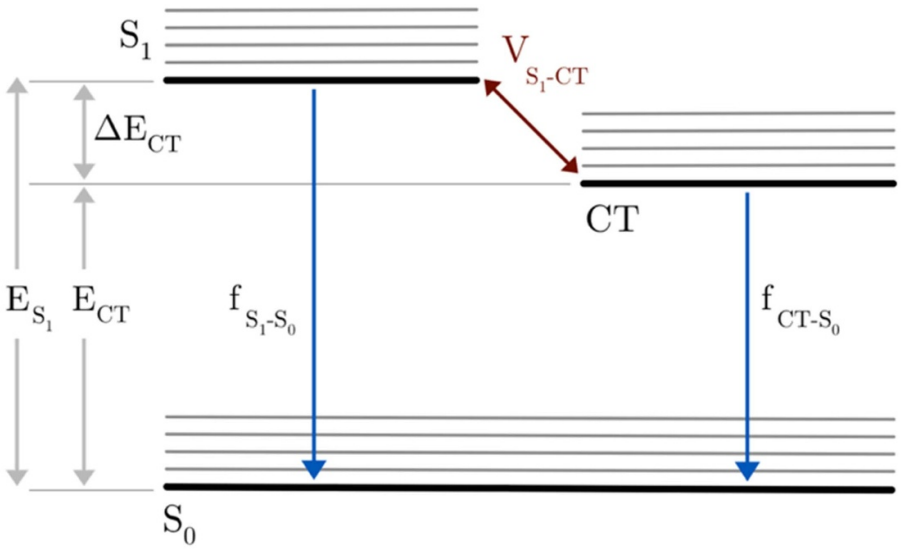

Figure 9. Schematic of the three-state models between the ground state (S_0), the singlet state (S_1) and the CT state. $V_{S1\text{-}CT}$ describes the coupling between the lowest singlet state and the CT state. The oscillator strengths of the S_1—S_0 and CT—S_0 transitions are described by $f_{S1\text{-}S0}$ and $f_{CT\text{-}S0}$ respectively. Reprinted with permission from [117]. Copyright (2019) American Chemical Society.

suggests that electronic coupling could increase the steepness of the low-energy absorption tail, thereby reducing radiative voltage losses.

A very recent publication [72] again by Chen *et al*, demonstrates further success of a three-state model and the importance of hybridization. The authors provide a unified framework for non-radiative voltage losses and demonstrate that fullerene-based blends behave as predicted by the energy gap law, while the behaviour of many low-loss NFA-based systems deviates from the energy gap law.

7. Conclusions

Losses in open-circuit voltage remain a major bottleneck to organic solar cell performance. The DB picture with a properly determined reference energy reliably quantifies voltage losses and classifies them into radiative and non-radiative contributions. It is thus well-suited to evaluate absorber blends in a comparative manner, e.g. for the purpose of assessing the photovoltaic quality of a novel absorber molecule. Compared to inorganic solar cell technologies, the existence of a CT state and the vibronic nature of transitions in organic molecules are responsible for high voltage losses in today's OSCs. Large vibrational energies broaden absorption and emission spectra, i.e. increase radiative losses, and facilitate non-radiative transitions without the need of an intermediate trap state as is the case for inorganic solar cells [149]. Successfully moving the CT state closer to the lowest lying singlet reduced radiative voltage losses from 100 s of mV to 10 s of mV for the most efficient NFA-based blends [47, 71]. As for inorganic solar cells, non-radiative losses now dominate in today's OSCs and typically exceed 200 mV [25, 47, 71] with the lowest non-radiative losses reached with NFAs.

Deeper insights into the causes of radiative and non-radiative losses requires analysis of the transition rates between ground and CT state, which includes—but is not limited to—determining the energy of the CT state. In this review, we describe the current state of analysing CT states and voltage losses in OSCs. Departing from a basic Marcus model for CT transitions, different advanced models account for the quantized nature of vibrations, static energetic disorder, and hybridization between the CT and singlet state. More complex models generally rely on fewer approximations and capture the physical nature of OSCs better, but also contain more parameters, which, in simpler models, are combined into fewer effective parameters. In practice, the different models are used to fit or reproduce experimental absorption and emission spectra. Together with the statistical variation between samples, the details of the fitting procedure may affect the extracted values. Here, low-offset systems are particularly challenging to analyse properly. These uncertainties complicate the judgement of which model better represents the data. For this, we recommend the guiding principle of Occam's razor should be respected: 'if two models can explain the data, choose the simpler one', whereby over-parametrization and resulting large uncertainty in fit values are automatically avoided. It is paramount to check all underlying assumptions, such as validity of reciprocity relations, and to explicitly communicate these along with the details of analysis procedure and associated

uncertainties, which can be best determined through a sensitivity analysis, e.g. of the fitting range. An open science approach of making models and experimental data publicly available and easily accessible attached to their publication is hugely beneficial.

In this review we showed how important it is to identify an appropriate model for CT state properties as this not only provides in-depth understanding, but precise determination of model parameters also allows the targeted design of molecules or blend microstructure. Further evidence on the viability of a certain model may come from computational simulations, targeted variations of the absorber blend, and additional experiments, such as transient absorption spectroscopy or microstructure probing. It cannot be expected that one model best describes experimental data for all material systems and experimental conditions. The scientific question is to classify material systems according to the appropriate CT model and to relate this to the molecular properties.

Looking forward, with the advent of low-offset systems, three-state models accounting for hybridization are becoming increasingly important to model efficient OSCs. Here, a simpler framework, ideally based on verifiable approximation, that is widely applicably to experimental data without the need computational simulations while retaining physical meaning would be beneficial. The role of static disorder as a source for spectral broadening in different material systems needs to be clarified and related to microstructure and molecular properties. There is a need for further theoretical models that unify static disorder, quantized dynamic disorder, and hybridization. Huge potential lies in the better understanding and improvement of non-radiative voltage losses. Here, a recent publication demonstrated the need to incorporate the electron spin when considering non-radiative voltage losses [150]. Eventually, a reduction of non-radiative recombination via bimolecular processes may give greater importance to trap-assisted Shockley-Read-Hall and surface recombination, which are the prevailing loss mechanisms in high efficiency inorganic solar cells. Finally, the relation between CT state properties and other processes and parameters of organic solar cells should be clarified. Examples are the influence of CT state energy (rather than driving force) on exciton dissociation efficiency [151], the relation between CT state static disorder and disorder in charge transport, and the influence of the CT state on the OSC device parameters, ideality factor and fill factor. There are still many processes to be better understood, and their understanding might resume previous achievements and pave the way to a further reduction of voltage losses and increase of PCE of this renewable energy technology.

Data availability statement

The data that support the findings of this study are available upon reasonable request from the authors.

Acknowledgments

A J acknowledges funding from the Wolfson-Marriott Graduate Scholarship from Wolfson College, Oxford. In addition, A J acknowledges funding from the EPRSC Doctoral Training Accounts and the Department of Physics at the University of Oxford. P K and M R acknowledge funding from the Global Challenges Research Fund (GCRF) through Science & Technology Facilities Council (STFC), Grant No. ST/R002754/1: Synchrotron Techniques for African Research and Technology (START).

ORCID iDs

Anna Jungbluth https://orcid.org/0000-0002-9888-6262
Pascal Kaienburg https://orcid.org/0000-0003-3887-3395
Moritz Riede https://orcid.org/0000-0002-5399-5510

References

[1] Chamberlain G A 1983 Organic solar cells: a review *Sol. Cells* **8** 47–83
[2] Brabec C J, Sariciftci N S and Hummelen J C 2001 Plastic solar cells *Adv. Funct. Mater.* **11** 15–26
[3] Tang W 1986 Two-layer organic photovoltaic cell *Appl. Phys. Lett.* **48** 183–5
[4] Hiramoto M, Fujiwara H and Yokoyama M 1991 Three-layered organic solar cell with a photoactive interlayer of codeposited pigments *Appl. Phys. Lett.* **58** 1062–4
[5] Sariciftci N S, Braun D, Zhang C, Srdanov V I, Heeger A J, Stucky G and Wudl F 1993 Semiconducting polymer-buckminsterfullerene heterojunctions: diodes, hotodiodes, and photovoltaic cells *Appl. Phys. Lett.* **62** 585–7
[6] Qian D *et al* 2018 Design rules for minimizing voltage losses in high-efficiency organic solar cells *Nat. Mater.* **17** 703–9
[7] Kirchartz T, Kaienburg P and Baran D 2018 Figures of merit guiding research on organic solar cells *J. Phys. Chem.* C **122** 5829–43
[8] Kirchartz T and Rau U 2018 What makes a good solar cell? *Adv. Energy Mater.* **8** 1703385
[9] Mihailetchi V D, Blom P W M, Hummelen J C and Rispens M T 2003 Cathode dependence of the open-circuit voltage of polymer: fullerenebulk heterojunction solar cells *J. Appl. Phys.* **94** 6849–54

[10] Scharber M C, Mühlbacher D, Koppe M, Denk P, Waldauf C, Heeger A and Brabec C 2006 Design rules for donors in bulk-heterojunction solar cells—towards 10% energy-conversion efficiency *Adv. Mater.* **18** 789–94
[11] Scharber M C 2016 On the efficiency limit of conjugated polymer: fullerene-based bulk heterojunction solar cells *Adv. Mater.* **28** 1994–2001
[12] Wang Y, Qian D, Cui Y, Zhang H, Hou J, Vandewal K, Kirchartz T and Gao F 2018 Optical gaps of organic solar cells as a reference for comparing voltage losses *Adv. Energy Mater.* **8** 1801352
[13] Li W, Hendriks K H, Furlan A, Wienk M M and Janssen R A J 2015 High quantum efficiencies in polymer solar cells at energy losses below 0.6 eV *J. Am. Chem. Soc.* **137** 2231–4
[14] Vandewal K, Benduhn J and Nikolis V C 2018 How to determine optical gaps and voltage losses in organic photovoltaic materials *Sustain. Energy Fuels* **2** 538–44
[15] Karuthedath S *et al* 2021 Intrinsic efficiency limits in low-bandgap non-fullerene acceptor organic solar cells *Nat. Mater.* **20** 378–84
[16] Classen A, Chochos C L, Lüer L, Gregoriou V G, Wortmann J, Osvet A, Forberich K, McCulloch I, Heumüller T and Brabec C J 2020 The role of exciton lifetime for charge generation in organic solar cells at negligible energy-level offsets *Nat. Energy* **5** 711–9
[17] Vandewal K, Gadisa A, Oosterbaan W D, Bertho S, Banishoeib F, Van Severen I, Lutsen L, Cleij T J, Vanderzande D and Manca J V 2008 The relation between open-circuit voltage and the onset of photocurrent generation by charge-transfer absorption in polymer: fullerene bulk heterojunction solar cells *Adv. Funct. Mater.* **18** 2064–70
[18] Potscavage W J, Yoo S and Kippelen B 2008 Origin of the open-circuit voltage in multilayer heterojunction organic solar cells *Appl. Phys. Lett.* **93** 193308
[19] Tvingstedt K, Vandewal K, Gadisa A, Zhang F, Manca J and Inganäs O 2009 Electroluminescence from charge transfer states in polymer solar cells *J. Am. Chem. Soc.* **131** 11819–24
[20] Vandewal K, Tvingstedt K, Gadisa A, Inganäs O and Manca J V 2009 On the origin of the open-circuit voltage of polymer-fullerene solar cells *Nat. Mater.* **8** 904–9
[21] Vandewal K, Tvingstedt K, Gadisa A, Inganäs O and Manca J V 2010 Relating the open-circuit voltage to interface molecular properties of donor: acceptorbulk heterojunction solar cells *Phys. Rev.* B **81** 125204
[22] Willems R E M, Weijtens C H L, de Vries X, Coehoorn R and Janssen R A J 2019 Relating frontier orbital energies from voltammetry and photoelectron spectroscopy to the open-circuit voltage of organic solar cells *Adv. Energy Mater.* **9** 1803677
[23] Panda P, Veldman D, Sweelssen J, Bastiaansen J J A M, Langeveld-Voss B M W and Meskers S C J 2007 Charge transfer absorption for π-conjugated polymers and oligomers mixed with electron acceptors *J. Phys. Chem.* B **111** 5076–81
[24] Benduhn J *et al* 2017 Intrinsic non-radiative voltage losses in fullerene-based organic solar cells *Nat. Energy* **2** 17053
[25] Armin A *et al* 2021 A history and perspective of non-fullerene electron acceptors for organic solar cells *Adv. Energy Mater.* **11** 2003570
[26] Rau U, Blank B, Müller T C M and Kirchartz T 2017 Efficiency potential of photovoltaic materials and devices unveiled by detailed-balance analysis *Phys. Rev. Appl.* **7** 044016
[27] Rau U 2007 Reciprocity relation between photovoltaic quantum efficiency and electroluminescent emission of solar cells *Phys. Rev.* B **76** 085303
[28] Wurfel P 1982 The chemical potential of radiation *J. Phys.* C **15** 3967–85
[29] Kirchartz T, Ding K and Rau U 2016 Fundamental electrical characterization of thin-film solar cells *Advanced Characterization Techniques for Thin Film Solar Cells* (Weinheim: Wiley-VCH Verlag GmbH & Co. KGaA) pp 41–69
[30] Shrotriya V, Li G, Yao Y, Moriarty T, Emery K and Yang Y 2006 Accurate measurement and characterization of organic solar cells *Adv. Funct. Mater.* **16** 2016–23
[31] Goris L, Haenen K, Nesládek M, Wagner P, Vanderzande D, De Schepper L, D'haen J, Lutsen L and Manca J V 2005 Absorption phenomena in organic thin films for solar cell applications investigated by photothermal deflection spectroscopy *J. Mater. Sci.* **40** 1413–8
[32] Vandewal K *et al* 2014 Efficient charge generation by relaxed charge-transfer states at organic interfaces *Nat. Mater.* **13** 63–68
[33] Street R A, Song K W, Northrup J E and Cowan S 2011 Photoconductivity measurements of the electronic structure of organic solar cells *Phys. Rev.* B **83** 165207
[34] Zeiske S, Kaiser C, Meredith P and Armin A 2020 Sensitivity of sub-bandgap external quantum efficiency measurements of solar cells under electrical and light bias *ACS Photonics* **7** 256–64
[35] Holovskỳ J, Stuckelberger M, Finsterle T, Conrad B, Peter Amalathas A, Müller M and Haug F-J 2020 Towards quantitative interpretation of Fourier-transform photocurrent spectroscopy on thin-film solar cells *Coatings* **10** 820
[36] Vanecek M and Poruba A 2002 Fourier-transform photocurrent spectroscopy of microcrystalline silicon for solar cells *Appl. Phys. Lett.* **80** 719–21
[37] Müller T C M and Kirchartz T 2016 Absorption and photocurrent spectroscopy with high dynamic range *Advanced Characterization Techniques for Thin Film Solar Cells* (Weinheim: Wiley-VCH Verlag GmbH & Co. KGaA) pp 189–214
[38] Jackson W B, Amer N M, Boccara A C and Fournier D 1981 Photothermal deflection spectroscopy and detection *Appl. Opt.* **20** 1333
[39] Melskens J, van Elzakker G, Li Y and Zeman M 2008 Analysis of hydrogenated amorphous silicon thin films and solar cells by means of Fourier transform photocurrent spectroscopy *Thin Solid Films* **516** 6877–81
[40] Puspitosari N, Longeaud C, Lachaume R, Zeyu L, Rusli R and Cabarrocas P R I 2017 Comparison of FTPS performed on thin films and solar cells *Phys. Status Solidi* c **14** 1700165
[41] Vanecek M, Kocka J, Stuchlik J and Triska A 1981 Direct measurement of the gap states and band tail absorption by constant photocurrent method in amorphous silicon *Solid State Commun.* **39** 1199–202
[42] Kirchartz T, Huhn V, Gerber A, Pieters B E and Rau U 2016 Electroluminescence analysis of solar cells and solar modules *Advanced Characterization Techniques for Thin Film Solar Cells* (Weinheim: Wiley-VCH Verlag GmbH & Co. KGaA) pp 71–92
[43] Wetzelaer G J A H, Kuik M and Blom P W M 2012 Identifying the nature of charge recombination in organic solar cells from charge-transfer state electroluminescence *Adv. Energy Mater.* **2** 1232–7
[44] Arneson C, Huang X, Huang X, Fan D, Gao M, Ye L, Ade H, Li Y and Forrest S R 2021 Relationship between charge transfer state electroluminescence and the degradation of organic photovoltaics *Appl. Phys. Lett.* **118** 063301
[45] Tvingstedt K, Vandewal K, Zhang F and Inganäs O 2010 On the dissociation efficiency of charge transfer excitons and Frenkel excitons in organic solar cells: a luminescence quenching study *J. Phys. Chem.* C **114** 21824–32
[46] Unold T and Gütay L 2016 Photoluminescence analysis of thin-film solar cells *Advanced Characterization Techniques for Thin Film Solar Cells* (Weinheim: Wiley-VCH Verlag GmbH & Co. KGaA) pp 275–97

[47] Perdigón-Toro L, Phuong L Q, Zeiske S, Vandewal K, Armin A, Shoaee S and Neher D 2021 Excitons dominate the emission from PM6: y6Solar cells, but this does not help the open-circuit voltage of the device *ACS Energy Lett.* **6** 557–64
[48] Baran D, Li N, Breton A-C, Osvet A, Ameri T, Leclerc M and Brabec C J 2014 Qualitative analysis of bulk-heterojunction solar cells without device fabrication: an elegant and contactless method *J. Am. Chem. Soc.* **136** 10949–55
[49] Fox M 2010 *Optical Properties of Solids* 2nd edn (Oxford: Oxford University Press)
[50] Cody G D, Wronski C R, Abeles B, Stephens R B and Brooks B 1980 Optical characterization of amorphous silicon hybride films *Solar Cells* **2** 227–43
[51] Kirchartz T, Abou-Ras D and Rau U 2016 Introduction to thin-film photovoltaics *Advanced Characterization Techniques for Thin Film Solar Cells* (Weinheim: Wiley-VCH Verlag GmbH & Co. KGaA) 1–40
[52] Burkhard G F, Hoke E T and McGehee M D 2010 Accounting for interference, scattering, and electrode absorption to make accurate internal quantum efficiency measurements in organic and other thin solar cells *Adv. Mater.* **22** 3293–7
[53] Bridgman P W 1928 Note on the principle of detailed balancing *Phys. Rev.* **31** 101–2
[54] Stolterfoht M *et al* 2019 The impact of energy alignment and interfacial recombination on the internal and external open-circuit voltage of perovskite solar cells *Energy Environ. Sci.* **12** 2778–88
[55] Donolato C 1985 A reciprocity theorem for charge collection *Appl. Phys. Lett.* **46** 270–2
[56] Smestad G and Ries H 1992 Luminescence and current-voltage characteristics of solar cells and optoelectronic devices *Sol. Energy Mater Sol. Cells* **25** 51–71
[57] Ross R T 1967 Some thermodynamics of photochemical systems *J. Chem. Phys.* **46** 4590–3
[58] Wang X and Lundstrom M S 2013 On the use of Rau's reciprocity to deduce external radiative efficiency in solar cells *IEEE J. Photovolt.* **3** 1348–53
[59] Müller T C M, Pieters B E, Kirchartz T, Carius R and Rau U 2014 Effect of localized states on the reciprocity between quantum efficiency and electroluminescence in Cu(In,Ga)Se2 and Si thin-film solar cells *Sol. Energy Mater. Sol. Cells* **129** 95–103
[60] Kirchartz T, Nelson J and Rau U 2016 Reciprocity between charge injection and extraction and its influence on the interpretation of electroluminescence spectra in organic solar cells *Phys. Rev. Appl.* **5** 054003
[61] Gong W, Faist M A, Ekins-Daukes N J, Xu Z, Bradley D D C, Nelson J and Kirchartz T 2012 Influence of energetic disorder on electroluminescence emission in polymer: fullerene solar cells *Phys. Rev.* B **86** 024201
[62] Armin A, Zarrabi N, Sandberg O J, Kaiser C, Zeiske S, Li W and Meredith P 2020 Limitations of charge transfer state parameterization using photovoltaic external quantum efficiency *Adv. Energy Mater.* **10** 2001828
[63] Yao J *et al* 2015 Quantifying losses in open-circuit voltage in solution-processable solar cells *Phys. Rev. Appl.* **4** 014020
[64] Rau U 2012 Superposition and reciprocity in the electroluminescence and photoluminescence of solar cells *IEEE J. Photovolt.* **2** 169–72
[65] Lupton J M 2002 Frequency up-conversion as a temperature probe of organic opto-electronic devices *Appl. Phys. Lett.* **80** 186–8
[66] Almora O, Cabrera C I, Garcia-Cerrillo J, Kirchartz T, Rau U and Brabec C J 2021 Quantifying the absorption onset in the quantum efficiency of emerging photovoltaic devices *Adv. Energy Mater.* **11** 2100022
[67] Almora Osbel *et al* 2021 Device performance of emerging photovoltaic materials (Version 1) *Adv. Energy Mater.* **11** 2002774
[68] Kaienburg P, Rau U and Kirchartz T 2016 Extracting information about the electronic quality of organic solar-cell absorbers from fill factor and thickness *Phys. Rev. Appl.* **6** 024001
[69] Shockley W and Queisser H J 1961 Detailed balance limit of efficiency of p-n junction solar cells *J. Appl. Phys.* **32** 510–9
[70] Liu Q *et al* 2020 18% Efficiency organic solar cells *Sci. Bull.* **65** 272–5
[71] Azzouzi M, Kirchartz T and Nelson J 2019 Factors controlling open-circuit voltage losses in organic solar cells *Trends Chem.* **1** 49–62
[72] Chen X-K *et al* 2021 A unified description of non-radiative voltage losses in organic solar cells *Nat. Energy* **6** 799–806
[73] Azzouzi M, Yan J, Kirchartz T, Liu K, Wang J, Wu H and Nelson J 2018 Nonradiative energy losses in bulk-heterojunction organic photovoltaics *Phys. Rev.* X **8** 031055
[74] Marcus R A 1957 On the theory of oxidation-reduction reactions involving electron transfer II. Applications to data on the rates of isotopic exchange reactions *J. Chem. Phys.* **26** 867–71
[75] Marcus R A 1956 On the theory of oxidation-reduction reactions involving electron transfer I *J. Chem. Phys.* **24** 966–78
[76] Marcus R A 1993 Electron transfer reactions in chemistry. Theory and experiment *Rev. Mod. Phys.* **65** 599–610
[77] Clarke T M and Durrant J R 2010 Charge photogeneration in organic solar cells *Chem. Rev.* **110** 6736–67
[78] Tress W 2014 *Organic Solar Cells* vol 208 (Cham: Springer International Publishing)
[79] May V and Kühn O 2011 *Charge and Energy Transfer Dynamics in Molecular Systems* (Weinheim: Wiley-VCH Verlag GmbH & Co. KGaA) (https://doi.org/10.1002/9783527633791)
[80] Jortner J 1976 Temperature dependent activation energy for electron transfer between biological molecules *J. Chem. Phys.* **64** 4860–7
[81] Unger T, Wedler S, Kahle F J, Scherf U, Bässler H and Köhler A 2017 The impact of driving force and temperature on the electron transfer in donor-acceptor blend systems *J. Phys. Chem.* C **121** 22739–52
[82] Kahle F J, Rudnick A, Bässler H and Köhler A 2018 How to interpret absorption and fluorescence spectra of charge transfer states in an organic solar cell *Mater. Horiz.* **5** 837–48
[83] Marcus R A 1964 Chemical and electrochemical electron-transfer theory *Annu. Rev. Phys. Chem.* **15** 155–96
[84] Marcus R A and Wardlaw D M 1986 Theory, experiment, and reaction rates. A personal view *J. Phys. Chem.* **90** 3460–5
[85] Atxabal A, Arnold T, Parui S, Hutsch S, Zuccatti E, Llopis R, Cinchetti M, Casanova F, Ortmann F and Hueso L E 2019 Tuning the charge flow between Marcus regimes in an organic thin-film device *Nat. Commun.* **10** 2089
[86] Coffey D C, Larson B W, Hains A W, Whitaker J B, Kopidakis N, Boltalina O V, Strauss S H and Rumbles G 2012 An optimal driving force for converting excitons into free carriers in excitonic solar cells *J. Phys. Chem.* C **116** 8916–23
[87] Ihly R, Mistry K S, Ferguson A J, Clikeman T T, Larson B W, Reid O, Boltalina O V, Strauss S H, Rumbles G and Blackburn J L 2016 Tuning the driving force for exciton dissociation in single-walled carbon nanotube heterojunctions *Nat. Chem.* **8** 603–9
[88] Yuan L, Wang L, Garrigues A R, Jiang L, Annadata H V, Anguera Antonana M, Barco E and Nijhuis C A 2018 Transition from direct to inverted charge transport Marcus regions in molecular junctions via molecular orbital gating *Nat. Nanotechnol.* **13** 322–9
[89] Benson-Smith J J, Goris L, Vandewal K, Haenen K, Manca J, Vanderzande D, Bradley D and Nelson J 2007 Formation of a ground-state charge-transfer complex in polyfluorene/[6,6]- phenyl-C61 butyric acid methyl ester (PCBM) blend films and its role in the function of polymer/PCBM solar cells *Adv. Funct. Mater.* **17** 451–7
[90] Guldi D M and Prato M 2000 Excited-state properties of C60 fullerene derivatives *Acc. Chem. Res.* **33** 695–703

[91] Hoke E T, Vandewal K, Bartelt J A, Mateker W R, Douglas J D, Noriega R, Graham K R, Fréchet J M J, Salleo A and McGehee M D 2013 Recombination in polymer: fullerene solar cells with open-circuit voltages approaching and exceeding 1.0 V *Adv. Energy Mater.* **3** 220–30
[92] Burke T M, Sweetnam S, Vandewal K and McGehee M D 2015 Beyond Langevin recombination: how equilibrium between free carriers and charge transfer states determines the open-circuit voltage of organic solar cells *Adv. Energy Mater.* **5** 1500123
[93] Göhler C, Saladina M, Wang Y, Spoltore D, Benduhn J, Leo K and Deibel C 2021 Temperature-dependent charge-transfer-state absorption and emission reveal the dominant role of dynamic disorder in organic solar cells *Phys. Rev. Appl.* **15** 064009
[94] Tvingstedt K, Benduhn J and Vandewal K 2020 Temperature dependence of the spectral line-width of charge-transfer state emission in organic solar cells; Static: vs. dynamic disorder *Mater. Horiz.* **7** 1888–900
[95] Vandewal K *et al* 2017 Absorption tails of donor: c60 blends provide insight into thermally activated charge-transfer processes and polaron relaxation *J. Am. Chem. Soc.* **139** 1699–704
[96] Meerheim R, Furno M, Hofmann S, Lüssem B and Leo K 2010 Quantification of energy loss mechanisms in organic light-emitting diodes *Appl. Phys. Lett.* **97** 253305
[97] Goushi K, Yoshida K, Sato K and Adachi C 2012 Organic light-emitting diodes employing efficient reverse intersystem crossing for triplet-to-singlet state conversion *Nat. Photon.* **6** 253–8
[98] Liu X, Wei F and Liu H 2009 Spectrum study of top-emitting organic light-emitting devices with micro-cavity structure *J. Semiconduct.* **30** 044007
[99] Puzzo D P, Helander M G, O'Brien P G, Wang Z, Soheilnia N, Kherani N, Lu Z and Ozin G A 2011 Organic light-emitting diode microcavities from transparent conducting metal oxide photonic crystals *Nano Lett.* **11** 1457–62
[100] Wittmann H E, Grüner J, Friend R H, Spencer G W C, Moratti S C and Holmes A B 1995 Microcavity effect in a single-layer polymer light-emitting diode *Adv. Mater.* **7** 541–4
[101] Kovačič M, Will P-A, Lipovšek B, Topič M, Lenk S, Reineke S and Krč J 2018 Coupled optical modeling for optimization of organic light-emitting diodes with external out coupling structures *ACS Photonics* **5** 422–30
[102] Salinas J F, Yip H L, Chueh C C, Li C Z, Maldonado J L and Jen A K Y 2012 Optical design of transparent thin metal electrodes to enhance in-coupling and trapping of light in flexible polymer solar cells *Adv. Mater.* **24** 6362–7
[103] Dahan N, Jehl Z, Hildebrandt T, Greffet J-J, Guillemoles J-F, Lincot D and Naghavi N 2012 Optical approaches to improve the photocurrent generation in Cu(In,Ga)Se2 solar cells with absorber thicknesses down to 0.5 μm *J. Appl. Phys.* **112** 094902
[104] Zuo L, Chueh C-C, Xu Y-X, Chen K-S, Zang Y, Li C-Z, Chen H and Jen A K-Y 2014 Microcavity-enhanced light-trapping for highly efficient organic parallel tandem solar cells *Adv. Mater.* **26** 6778–84
[105] Yu W, Shen L, Meng F, Long Y, Ruan S and Chen W 2012 Effects of the optical microcavity on the performance of ITO-free polymer solar cells with WO 3/Ag/WO 3 transparent electrode *Sol. Energy Mater. Sol. Cells* **100** 226–30
[106] Long Y 2009 Improving optical performance of inverted organic solar cells by microcavity effect *Appl. Phys. Lett.* **95** 193301
[107] Sergeant N P, Hadipour A, Niesen B, Cheyns D, Heremans P, Peumans P and Rand B P 2012 Design of transparent anodes for resonant cavity enhanced light harvesting in organic solar cells *Adv. Mater.* **24** 728–32
[108] Lin H-W, Chiu S-W, Lin L-Y, Hung Z-Y, Chen Y-H, Lin F and Wong K-T 2012 Device engineering for highly efficient top-illuminated organic solar cells with microcavity structures *Adv. Mater.* **24** 2269–72
[109] Ullbrich S, Siegmund B, Mischok A, Hofacker A, Benduhn J, Spoltore D and Vandewal K 2017 Fast organic near-infrared photodetectors based on charge-transfer absorption *J. Phys. Chem. Lett.* **8** 5621–5
[110] Siegmund B *et al* 2017 Organic narrowband near-infrared photodetectors based on intermolecular charge-transfer absorption *Nat. Commun.* **8** 15421
[111] List M, Sarkar T, Perkhun P, Ackermann J, Luo C and Würfel U 2018 Correct determination of charge transfer state energy from luminescence spectra in organic solar cells *Nat. Commun.* **9** 3631
[112] Kaiser C, Zeiske S, Meredith P and Armin A 2020 Determining ultralow absorption coefficients of organic semiconductors from the sub-bandgap photovoltaic external quantum efficiency *Adv. Opt. Mater.* **8** 1901542
[113] Karki A, Vollbrecht J, Dixon A L, Schopp N, Schrock M, Reddy G N M and Nguyen T-Q 2019 Understanding the high performance of over 15% efficiency in single-junction bulk heterojunction organic solar cells *Adv. Mater.* **31** 1903868
[114] Perdigón-toro L *et al* 2020 Barrierless free charge generation in the high-performance PM6:Y6 bulk heterojunction non-fullerene solar cell *Adv. Mater.* **32** 1906763
[115] Hou J, Inganas O, Friend R H and Gao F 2018 Organic solar cells based on non-fullerene acceptors *Nat. Mater.* **17** 119–28
[116] Menke S M, Ran N A, Bazan G C and Friend R H 2018 Understanding energy loss in organic solar cells: toward a new efficiency regime *Joule* **2** 25–35
[117] Eisner F D, Azzouzi M, Fei Z, Hou X, Anthopoulos T D, Dennis T J S, Heeney M and Nelson J 2019 Hybridization of local exciton and charge-transfer states reduces nonradiative voltage losses in organic solar cells *J. Am. Chem. Soc.* **141** 6362–74
[118] Kawashima K, Tamai Y, Ohkita H, Osaka I and Takimiya K 2015 High-efficiency polymer solar cells with small photon energy loss *Nat. Commun.* **6** 10085
[119] Baran D *et al* 2016 Reduced voltage losses yield 10% efficient fullerene free organic solar cells with >1 V open circuit voltages *Energy Environ. Sci.* **9** 3783–93
[120] Cheng P, Zhang M, Lau T-K, Wu Y, Jia B, Wang J, Yan C, Qin M, Lu X and Zhan X 2017 Realizing small energy loss of 0.55 eV, high open-circuit voltage >1 V and high efficiency >10% in fullerene-free polymer solar cells via energy driver *Adv. Mater.* **29** 1605216
[121] Ran N A *et al* 2016 Harvesting the full potential of photons with organic solar cells *Adv. Mater.* **28** 1482–8
[122] Li T-Y, Benduhn J, Li Y, Jaiser F, Spoltore D, Zeika O, Ma Z, Neher D, Vandewal K and Leo K 2018 Boron dipyrromethene (BODIPY) with: meso -perfluorinated alkyl substituents as near infrared donors in organic solar cells *J. Mater. Chem.* A **6** 18583–91
[123] Nikolis V C *et al* 2020 Field effect versus driving force: charge generation in small-molecule organic solar cells *Adv. Energy Mater.* **10** 2002124
[124] Benduhn J 2019 Intermolecular charge-transfer states in organic optoelectronic devices Technische Universität Dresden
[125] Coropceanu V, Cornil J, Da Silva Filho D A, Olivier Y, Silbey R and Brédas J L 2007 Charge transport in organic semiconductors *Chem. Rev.* **107** 926–52
[126] Brédas J L, Beljonne D, Coropceanu V and Cornil J 2004 Charge-transfer and energy-transfer processes in π-conjugated oligomers and polymers: a molecular picture *Chem. Rev.* **104** 4971–5003
[127] Köhler A and Bässler H 2015 *Electronic Processes in Organic Semiconductors* (Weinheim: Wiley-VCH Verlag GmbH & Co. KGaA) (https://doi.org/10.1002/9783527685172)

[128] Fuchs F, Schmitt S, Walter C, Engels B, Herzig E M, Müller-Buschbaum P, Dyakonov V and Deibel C 2017 Vibrational spectroscopy of a low-band-gap donor-acceptor copolymer and blends *J. Phys. Chem.* C **121** 19543–7
[129] Jortner J, Verhoeven J W, Phys Chem T J J and Chem Phys P F J 1994 Lifetimes for radiative charge recombination in donor-acceptor molecules *J. Am. Chem. Soc.* **116** 7349–55 (UTC)
[130] Newton M D 1991 Quantum chemical probes of electron-transfer kinetics: the nature of donor-acceptor interactions *Chem. Rev.* **91** 767–92
[131] Hsu C P 2009 The electronic couplings in electron transfer and excitation energy transfer *Acc. Chem. Res.* **42** 509–18
[132] Zhao Y and Liang W Z 2012 Charge transfer in organic molecules for solar cells: theoretical perspective *Chem. Soc. Rev.* **41** 1075–87
[133] Kastinen T, Da Silva Filho D A, Paunonen L, Linares M, Ribeiro Junior L A, Cramariuc O and Hukka T I 2019 Electronic couplings and rates of excited state charge transfer processes at poly(thiophene-: co -quinoxaline)-PC71BM interfaces: two- versus multi-state treatments *Phys. Chem. Chem. Phys.* **21** 25606–25
[134] Panhans M *et al* 2020 Molecular vibrations reduce the maximum achievable photovoltage in organic solar cells *Nat. Commun.* **11** 1488
[135] Yan J, Rezasoltani E, Azzouzi M, Eisner F and Nelson J 2021 Influence of static disorder of charge transfer state on voltage loss in organic photovoltaics *Nat. Commun.* **12** 3642
[136] Zheng Z, Tummala N R, Wang T, Coropceanu V and Brédas J L 2019 Charge-transfer states at organic–organic interfaces: impact of static and dynamic disorders *Adv. Energy Mater.* **9** 1803926
[137] Coropceanu V, Chen X K, Wang T, Zheng Z and Brédas J L 2019 Charge-transfer electronic states in organic solar cells *Nat. Rev. Mater.* **4** 689–707
[138] Chen X K, Coropceanu V and Brédas J L 2018 Assessing the nature of the charge-transfer electronic states in organic solar cells *Nat. Commun.* **9** 5295
[139] Rand B P *et al* 2012 The impact of molecular orientation on the photovoltaic properties of a phthalocyanine/fullerene heterojunction *Adv. Funct. Mater.* **22** 2987–95
[140] Chen X K, Ravva M K, Li H, Ryno S M and Brédas J L 2016 Effect of molecular packing and charge delocalization on the nonradiative recombination of charge-transfer states in organic solar cells *Adv. Energy Mater.* **6** 1601325
[141] Brédas J L, Norton J E, Cornil J and Coropceanu V 2009 Molecular understanding of organic solar cells: the challenges *Acc. Chem. Res.* **42** 1691–9
[142] Lin Y H L, Fusella M A and Rand B P 2018 The impact of local morphology on organic donor/acceptor charge transfer states *Adv. Energy Mater.* **8** 1702816
[143] Belova V *et al* 2017 Evidence for anisotropic electronic coupling of charge transfer states in weakly interacting organic semiconductor mixtures *J. Am. Chem. Soc.* **139** 8474–86
[144] Panzer F, Bässler H and Köhler A 2017 Temperature induced order-disorder transition in solutions of conjugated polymers probed by optical spectroscopy *J. Phys. Chem. Lett.* **8** 114–25
[145] Ziffer M E *et al* 2018 Long-lived, non-geminate, radiative recombination of photogenerated charges in a polymer/small-molecule acceptor photovoltaic blend *J. Am. Chem. Soc.* **140** 9996–10008
[146] Joseph S, Ravva M K and Bredas J L 2017 Charge-transfer dynamics in the lowest excited state of a pentacene-fullerene complex: implications for organic solar cells *J. Phys. Chem. Lett.* **8** 5171–6
[147] D'Avino G, Muccioli L, Olivier Y and Beljonne D 2016 Charge separation and recombination at polymer-fullerene heterojunctions: delocalization and hybridization effects *J. Phys. Chem. Lett.* **7** 536–40
[148] Few S, Frost J M, Kirkpatrick J and Nelson J 2014 Influence of chemical structure on the charge transfer state spectrum of a polymer: fullerene complex *J. Phys. Chem.* C **118** 8253–61
[149] Kirchartz T, Markvart T, Rau U and Egger D A 2018 Impact of small phonon energies on the charge-carrier lifetimes in metal-halide perovskites *J. Phys. Chem. Lett.* **9** 939–46
[150] Gillett A J *et al* 2021 The role of charge recombination to triplet excitons in organic solar cells *Nature* **597** 666–71
[151] Collado-Fregoso E *et al* 2019 Energy-gap law for photocurrent generation in fullerene-based organic solar cells: the case of low-donor-content blends *J. Am. Chem. Soc.* **141** 2329–41